Submitted to the Astronomical Journal

Population Synthesis in the Blue III. The Integrated Spectrum of M67 and the Spectroscopic Age of M32

Ricardo P. Schiavon

UCO/Lick Observatory, University of California, Santa Cruz, CA 95064

ripisc@ucolick.org

Nelson Caldwell

Smithsonian Astrophysical Observatory, 60 Garden Street, Cambridge, MA 02138

caldwell@cfa.harvard.edu

James A. Rose

Department of Physics and Astronomy, CB 3255, University of North Carolina, Chapel Hill, NC 27599

jim@physics.unc.edu

ABSTRACT

We construct an integrated spectrum of the intermediate age, solar metallicity Galactic cluster M67, from individual spectroscopic observations of bona fide cluster members. The spectrum so obtained is used as a template to test our stellar population synthesis (SPS) models, in an age and metallicity regime where such models remain largely untested. As a result, we demonstrate that our models predict a spectroscopic age of 3.5 $\pm$ 0.5 Gyr for M67, which is the same age we obtain from fitting isochrones to the color-magnitude diagram of the cluster. Full consistency is reached when using either $H\beta$, $H\gamma$ or $H\delta$ as the age indicator. We also check if the models, when applied to the cluster integrated spectrum, predict elemental abundances in agreement with the known detailed abundance pattern of the cluster. The models also pass the latter test, by predicting the abundances of iron, magnesium, carbon and nitrogen in agreement with detailed abundance analyses of cluster stars to within 0.1 dex. Encouraged by the high degree of consistency of our models, we apply them to the study of the integrated

spectrum of the central 3" of the compact elliptical galaxy M32. The resulting luminosity-weighted age of the galaxy ranges between 2 and 3.5 Gyr, depending on the age indicator adopted. According to our models, the center of M32 seems to have a super-solar iron abundance, ranging between [Fe/H] $\sim +0.1$ and $+0.3$, depending on the spectral index adopted. The light element magnesium seems to be underabundant in the center of M32 relative to iron by about ~ 0.1–0.2 dex, whereas the data are consistent with nearly solar carbon and nitrogen abundances relative to iron. We find that single age, single metallicity stellar population models with a solar-scaled abundance pattern cannot fit all the Balmer and metal lines in the integrated spectrum of M32. In particular, there is a systematic trend in the sense that bluer absorption lines indicate a younger age and a higher metallicity. This slight inconsistency can be due either to (unaccounted for) abundance ratio effects on blue iron and Balmer line indices, or to a spread of the ages of the stellar populations in M32. Current stellar population models cannot break this degeneracy at the level of accuracy required to address this problem.

Subject headings: galaxies:stellar content–Galactic clusters:general–Galactic clusters:individual (M67)–galaxies:individual (M32)–stars:evolution

1. Introduction

With the commissioning of both wide field spectroscopic survey instruments (2dF, Colless et al. 2001; SDSS, York et al. 2000) and of deep multi-aperture spectroscopy on large aperture telescopes (e.g. DEEP survey, Davis et al. 2003, VIRMOS-VLT Deep survey, Le Fèvre et al. 2001), it is becoming increasingly important to reliably extract information concerning the stellar populations in galaxies from their integrated spectra.

Stellar population synthesis (SPS) provides the only tool to estimate the ages and metal abundances of stellar populations in distant, unresolved galaxies. The application of SPS models to the study of unresolved systems, however, needs to be preceded by extensive and detailed testing against the observations of nearby, resolved systems, for which the key stellar population (SP) parameters, such as age, metal abundances (i.e., metallicities and abundance ratios) and initial mass function (IMF) are known independently. To gain confidence that modelling of the integrated spectra of galaxies is sufficiently reliable to extract useful information about their luminosity-weighted mean ages and chemical compositions, it is often proposed that integrated light observations of star clusters should be used as a testing ground for the evolutionary synthesis models that form the backbone of integrated

light analysis. Recently, different groups have pursued this aim, by comparing SPS model predictions to the observations of globular clusters with a range of SP parameters (Leonardi & Rose 2003, Maraston et al. 2003, Beasley, Hoyle & Sharples 2002, Puzia et al. 2002, Schiavon et al. 2002a,b).

Given the extensive evidence in recent work that the integrated light of early-type galaxies is often dominated by intermediate-age stellar populations (e.g., Trager et al. 2000, Kuntschner 2000, Caldwell, Rose & Concannon 2003), it has become of fundamental importance that SPS models be tested in the regime of intermediate age ($\sim$ 4 Gyr) and solar metallicity. Moreover, this is the range of SP parameters expected in early-type galaxies at moderately high redshifts ($z \sim 1$). Most of the previous studies, however, have concentrated on Galactic globular clusters, thus being limited to ages older than $\sim$ 10 Gyr. More recently Leonardi & Rose (2003) and Beasley et al. (2002) have extended SPS model calibration efforts to younger ages by comparing model predictions to observations of clusters from the Large Magellanic Cloud. In general, good consistency was found between SPS ages and metallicities and those from the literature. However, the quality of cluster CMDs for age determinations, as well as the variety of isochrones used in the literature, make the precision and homogeneity of CMD ages for LMC clusters quite low, compared with what can be achieved with Galactic clusters. Moreover, it is difficult to check the metallicity scale of SP models using LMC clusters because they lack reliable metallicity determinations based on classical abundance analysis of high resolution spectra of stellar members. To this date, such conditions are met only for Galactic clusters, which makes them the ideal templates for the calibration of SP models.

In order to cure this deficiency, we constructed an integrated spectrum of M67, an old ($\sim$ 4 Gyr) Galactic open cluster with solar metallicity. The latter spectrum is used as a template for the calibration of the SPS models in the regime of intermediate age and solar metallicity. Our integrated spectrum was constructed by observing individual bona fide cluster members and coadding their spectra weighting according to their magnitudes and an assumed IMF.

We present a detailed comparison of our SPS models to the above integrated spectrum of M67. We find that our model spectroscopic ages based on all Balmer lines from $H\beta$ through $H\delta$ agree with the CMD-based cluster age to within 0.5 Gyr. We also verify whether the models correctly predict elemental abundances from integrated spectra, by comparing to the well known abundances of M67 stars, taken from the literature. Again, our models pass the test by predicting correctly the abundances of key elements, like magnesium, carbon and nitrogen.

Our spectrum of M67 is also compared with an integrated spectrum of the central 3”

of M32, obtained with the same instrumental setup. We find that the two spectra look remarkably alike, indicating that the luminosity-weighted age and metal abundances of M32 are likely to be very close to those of M67.

The above results encouraged us to compare our model predictions to the integrated spectrum of another benchmark of stellar population studies, the compact elliptical galaxy M32. The resulting spectroscopic age is somewhere between 2 and 3.5 Gyr, depending on the Balmer line adopted in the analysis. Also depending on the iron feature used, the mean iron abundance of M32 results slightly above solar, or strongly super-solar. Analysis of other features, like Mgb and CN bands, shows that magnesium is underabundant relative to iron in the center of M32, while carbon and nitrogen have about solar abundance ratios relative to iron.

In Section 2 we describe the selection of our sample of M67 members and the observations. In Section 3 we describe the computation of the integrated spectrum of M67. In Section 4, a brief description of the models is presented, and they are compared with both the CMD and the integrated spectrum of M67. The analysis of the integrated spectrum of M32 is presented in Section 5, and in Section 6 we summarize our conclusions.

2. Observational Data

2.1. Sample Selection

2.1.1. M67 Stars

To obtain a representative integrated spectrum of M67 built up from observations of individual stars in the cluster, spectra and photometry covering the entire CMD from the tip of the giant branch through the lower main sequence are required. Included as well must be giant branch (GB) "clump" stars, i.e., the core helium burning phase, as well as blue straggler (BS) stars. As a starting point, we used the CMD of Montgomery, Marschall, & Janes (1993; hereafter MMJ) to produce a candidate list of 103 stars covering the CMD from the tip of the giant branch down to 1.5 mag below the main sequence turnoff (MSTO, V$\sim$14), as well as several GB clump stars and a number of BS stars. The stars were selected for observation strictly on the basis of their positions in the CMD. The cutoff at the fainter MS magnitudes is imposed by the combination of required spectral resolution and S/N ratio. As decribed below, we filled in the lower MS with observations of solar-abundance field dwarfs.

Naturally, there will be interlopers potentially contaminating the true M67 cluster members. We use four methods to filter out such interlopers. The first is to search for proper

motion non-members, based on the study carried out by Sanders (1977). We find 16 stars in our sample with a proper-motion membership probability of 30% or less. A second criterion is radial velocity. In addition to our own velocities, which have a 1-σ accuracy of $\pm$11 km/s, many of our stars are observed by either Mathieu et al. (1986), with a precision of better than 1 km/s, and by Scott, Friel, & Janes (1995), with a precision similar to ours. We find that 13 stars have radial velocities inconsistent with membership in M67; six of these stars overlap with the proper motion non-members.

A third way to discover non-members is if the metal-abundance of the star is inconsistent with the near-solar composition of M67. Specifically, the MSTO color of M67 is similar to that of the Galactic thick disk population (Carney, Latham & Laird 1989; Gilmore, Wyse & Jones 1995). In addition, M67 is located approximately 0.5 kpc above the Galactic plane, and thus at the distance where one can expect significant contamination from the thick disk MSTO. To identify thick disk MSTO stars, we measure the Lick Fe5270 and Hβ indices (Worthey et al. 1994) for all of the stars in our sample, then find a mean relation between Fe5270 and Hβ. Stars that deviate by more than –0.4 Å in Fe5270, for their Hβ, are deemed to be metal-weak, with the threshold at –0.4 Å determined from the fit to Hβ versus [Fe/H] given in Worthey et al. (1994). Altogether we find six stars in the M67 turnoff region which are metal-poor. Five of these stars are proper motion non-members, and three of the stars are further confirmed as radial velocity non-members. Given that the majority of stars in our list are indeed cluster members, it is suggestive that the proper motion and radial velocity non-members that we find in the turnoff region are also systematically metal-poor. Thus we conclude that there is significant contamination of the observed CMD of M67 with thick disk turnoff stars.

A fourth way to detect non-members is by identifying stars with anomalous positions in the M67 CMD based on their inferred absolute V magnitude, assuming membership in M67, and comparing to distances inferred from their surface gravities. Here we make use of a pair of spectral indices, Sr IIλ4077/Fe Iλ4045 and $H\delta$/Fe Iλ4045, that have been utilized by Rose (1984; 1985a,b) to discriminate surface gravity in stars. Briefly, the method relies on the gravity sensitivity of the ionization balance between singly ionized strontium and neutral iron, with the temperature sensitivity moderated by the strength of $H\delta$. Using this procedure we find five stars with anomalous CMD positions, three of which are proper motion and/or radial velocity non-members as well. The five cases are as follows. The star MMJ6496 is positioned at V=11.26 and $(B-V)$=0.62 in the CMD, thus is located at low surface gravity if it is indeed a member of M67, and at an unusual location, i.e., well above the MSTO, but too red for a BS star. However, the surface gravity determined from the Sr IIλ4077/Fe Iλ4045 index indicates that it is a dwarf, and its Fe5270 index indicates solar composition. Thus it appears to be a relatively nearby ($\sim$ 200 pc away) solar composition thin disk dwarf. The

star MMJ5336 has V=12.96, $(B-V)$=1.11, placing it in an anomalously red region of the bottom of the SGB. Its spectral characteristis are all consistent with a cool thick disk (i.e., metal-poor) giant. The star MMJ6034 has similar characteristics to MMJ5336. In contrast, the stars MMJ5571 and MMJ5688 have the problem of lying blueward in color of the MSTO. MMJ5571 has V=12.65 and $(B-V)$=0.52, while MMJ5688 has V=12.89 and $(B-V)$=0.45. For both of these stars the Sr IIλ4077/Fe Iλ4045 index indicates low surface gravity.

We have summarized the case for the non-member stars in Table 1, where stellar IDs (following the nomenclature of MMJ), coordinates, magnitudes and colors are listed together with the criteria used to decide the non-membership of each star. In Table 2 we list the stars found to be members of M67, which were used to construct the integrated spectrum of the cluster. In Figure 1 we display the M67 bona fide member stars in the color-magnitude diagram.

Table 1. Stars which were found *not* to be members of M67

ID (MMJ#)	RA(2000)	Dec(2000)	V	$(B-V)$	Criteria[a]
6474	8 50 21.1	12 21 11.5	10.520	1.230	2
6511	8 51 56.0	11 51 26.4	10.600	0.340	1
6508	8 52 10.9	11 31 49.3	10.930	1.150	1
6496	8 51 46.0	11 36 18.6	11.260	0.620	1,2,4
5877	8 51 30.4	11 48 57.6	12.110	1.006	2
6090	8 51 42.6	11 46 36.4	12.368	0.581	1,2,3
5124	8 50 41.5	11 44 30.0	12.374	0.746	1,3
6293	8 51 58.5	11 46 52.7	12.429	0.618	1,3
5451	8 51 07.2	11 53 01.6	12.595	0.637	3
5348	8 51 00.8	11 39 37.5	12.620	0.721	1
5571	8 51 15.4	11 47 31.3	12.651	0.517	4
5624	8 51 17.9	11 45 54.1	12.730	0.554	2
5239	8 50 51.7	11 48 10.1	12.846	0.501	1
5864	8 51 29.4	11 54 13.6	12.868	0.603	2
5688	8 51 20.5	11 46 16.2	12.891	0.448	4
6034	8 51 37.9	11 58 49.0	12.911	1.000	1,4
5336	8 50 59.7	11 39 22.2	12.964	1.107	1,2,4
5222	8 50 50.7	11 35 03.0	12.988	0.540	1,2,3
6172	8 51 50.6	11 36 33.8	13.419	0.445	1,2
5434	8 51 07.4	11 36 53.5	13.422	0.541	2
6430	8 52 13.4	11 46 01.1	13.457	0.514	2
5763	8 51 24.1	11 47 09.4	13.477	0.614	1
6467	8 52 16.6	11 42 29.8	13.517	0.536	1
5600	8 51 17.6	11 39 36.0	13.562	0.567	1
5257	8 50 53.4	11 40 43.5	13.726	0.609	1,2,3
6009	8 51 36.3	11 56 50.5	14.001	0.617	2

[a]Reasons for determination of non-membership: 1 = proper motion; 2 = radial velocity; 3 = metallicity; 4 = position in CMD

Table 2. Stars which were found to be members of M67, and were used in the construction of the cluster integrated spectrum

ID (MMJ#)	RA(1950)	Dec(1950)	V	$(B-V)$
6395	8 49 25.57	11 58 05.5	14.036	0.615
5249	8 48 09.05	11 51 17.9	13.703	0.561
5583	8 48 32.24	11 55 49.8	13.491	0.630
6134	8 49 02.38	11 57 45.2	13.381	0.572
5342	8 48 14.97	12 07 52.5	13.265	0.575
5741	8 48 38.86	12 00 30.4	13.260	0.464
5795	8 48 41.37	12 03 56.3	13.259	0.619
5716	8 48 37.99	11 57 58.2	13.183	0.581
5679	8 48 36.28	11 57 09.6	13.145	0.566
5169	8 48 02.00	11 54 21.7	13.117	0.542
5855	8 48 45.32	11 56 45.3	12.934	0.917
6114	8 49 00.70	11 58 04.5	12.934	0.919
5228	8 48 05.79	12 00 28.3	12.931	0.851
6259	8 49 12.03	12 01 33.9	12.920	0.983
5969	8 48 50.19	12 01 01.7	12.909	0.534
6169	8 49 04.65	12 08 10.1	12.906	0.970
5688	8 48 36.52	11 57 33.6	12.891	0.448
6408	8 49 27.32	11 56 57.3	12.889	0.817
5318	8 48 13.96	12 03 38.2	12.862	0.941
5284	8 48 10.12	12 07 44.4	12.844	0.522
5756	8 48 39.74	11 58 33.4	12.835	0.783
5586	8 48 31.59	12 04 15.7	12.831	0.567
5996	8 48 51.19	12 09 14.6	12.826	0.775
5118	8 47 56.63	11 59 00.8	12.818	0.521
5248	8 48 07.54	12 08 11.0	12.803	0.547
6313	8 49 15.49	12 04 16.9	12.790	0.584
5833	8 48 44.05	12 00 45.0	12.784	0.487
5350	8 48 15.96	12 05 48.0	12.782	0.813
5927	8 48 48.33	11 59 19.0	12.777	0.822
6107	8 48 59.97	11 57 42.9	12.750	0.758
5362	8 48 16.91	12 01 27.1	12.725	0.739

Table 2—Continued

ID (MMJ#)	RA(1950)	Dec(1950)	V	$(B-V)$
5993	8 48 51.97	11 57 51.6	12.722	0.683
5059	8 47 52.01	11 54 30.2	12.712	0.913
5191	8 48 03.55	11 56 05.6	12.700	0.482
6228	8 49 08.23	12 15 41.8	12.688	0.622
5853	8 48 44.67	12 03 17.6	12.677	0.684
5571	8 48 31.36	11 58 48.4	12.651	0.517
5929	8 48 48.38	11 59 10.2	12.648	0.617
5041	8 47 50.31	11 51 11.4	12.629	0.594
5643	8 48 34.61	11 58 19.8	12.596	0.783
5451	8 48 23.04	12 04 18.3	12.595	0.637
5790	8 48 41.30	11 58 51.7	12.533	0.589
6089	8 48 58.36	12 01 10.3	12.514	0.598
6158	8 49 04.22	12 02 30.6	12.505	0.663
5544	8 48 29.47	12 01 54.9	12.286	0.676
5699	8 48 37.17	11 57 09.9	12.260	0.569
5997	8 48 51.62	12 04 52.9	12.230	0.993
5667	8 48 35.84	11 58 17.5	12.126	0.458
6477	8 48 11.49	12 03 30.3	12.04	0.60
6502	8 48 58.23	12 01 26.0	11.63	1.05
6484	8 48 23.70	11 59 25.7	11.55	0.41
6488	8 48 39.66	12 01 06.6	11.52	0.87
6505	8 48 58.23	12 02 41.3	11.33	1.07
6491	8 48 37.60	12 03 55.1	11.315	0.61
6489	8 48 32.90	12 02 03.4	11.20	1.08
6480	8 48 30.30	11 56 17.3	11.078	0.43
6501	8 48 48.51	12 00 09.9	11.063	0.19
6490	8 48 42.88	12 03 10.1	10.99	0.11
6497	8 48 59.52	11 55 44.9	10.76	1.13
6510	8 49 26.73	11 55 25.2	10.70	0.11
6492	8 48 28.53	12 03 59.1	10.59	1.12
6506	8 48 59.68	12 08 00.8	10.58	1.10

2.1.2. Lower Main Sequence Field Stars

With the instrumental setup available (see Section 2.2) we cannot easily go fainter than V=14, so we need to fill in the lower main sequence by observing field stars of roughly solar abundance. Since these later-type stars all have lifetimes in excess of the age of the Galaxy, they are consequently unevolved. Also, they will be seen to contribute only modestly to the integrated spectral indices in the blue. Thus we do not consider that using field stars as surrogates for M67 members in the K dwarf regime produces any serious concerns. The stars adopted re listed in Table 3, where the V magnitudes listed are not the stars' apparent magnitudes but rather the magnitudes they would have at the distance of M67. The latter were computed using the Hipparcos parallaxes of the field stars and the distance modulus of the cluster, discussed in Section 4.1.

2.1.3. Field M Giants

Due to the decreasing lifetime as a star ascends the GB, representation of the upper GB of M67 is sparse. To remedy this situation, we have observed a number of cool field M giants, which were selected among stars from the Jones (1999) spectral library, on the basis of the strength of TiO bands in their spectra. The stars adopted are listed in Table 3.

2.2. Observations

Stars in M67 were observed from 2002 January to April, using the FAST spectrograph (Fabricant et al 1998) on the 1.5m telescope of the Whipple Observatory. A 600 gpm grating was used with a 2" slit, which gave a spectral coverage from 3500 Å to 5500 Å, at a resolution of 2.7 Å and a dispersion of 0.75 Å pixel^{-1}. All observations were taken with the slit aligned with the parallactic angle. Exposure times ranged from a few seconds for the bright giants, to 30 minutes for main sequence stars. Spectra were extracted from the CCD images in the standard way using programs in IRAF, and flux calibrated using standard star spectra collected during the observing run. Non-photometric conditions and the relatively small slit meant that zero point of the flux calibration is not accurate, though the relative fluxes between wavelengths should be good to about 5%, based on the fits to all the spectrophotometric standard stars.

Bright field stars were observed with the same equipment and technique, to supply a library for the fainter main sequence stars, as well as M giants.

Table 2—Continued

ID (MMJ#)	RA(1950)	Dec(1950)	V	$(B-V)$
6512	8 49 15.35	12 06 24.0	10.55	1.10
6503	8 48 44.87	12 01 50.7	10.55	1.12
6494	8 48 42.01	12 05 09.4	10.48	1.10
6485	8 48 38.71	11 59 19.0	10.48	1.11
6516	8 49 34.57	11 55 46.7	10.47	1.12
6481	8 48 27.72	11 56 38.8	10.03	-0.073
6472	8 47 34.04	12 06 34.9	9.98	1.10

Table 3. Field Stars Included in the Construction of the Integrated Spectrum of M67. The V magnitudes listed are the apparent magnitudes these stars would have if they were at the distance of M67

ID	V	$(B-V)$	Spectral Type
HD61606A	16.055	1.00	K2V
HD136834	15.845	1.03	K3V
HD37216	15.175	0.78	G5
HD165341	15.105	0.90	K0V
HD69830	15.075	0.84	K0V
HD106156	15.055	0.83	G8V
HD128987	14.975	0.72	G6V
HD126511	14.865	0.94	G5
HD69582	14.675	0.74	G5
HD49178	14.495	0.70	G0
HD158614	13.835	0.76	G9IV-V
HD94705	9.445	1.25	M5.5III
HD62721	9.195	1.53	K4III
HD47914	9.135	1.54	K5III
HD70272	9.135	1.61	K4.5III
HD60522	9.125	1.57	M0III
HD98991	10.685	0.45	F3IV

We also obtained a spectrum of M32 using the same instrumental setup as above, but adopting a 3" slit width. The integrated spectrum was obtained through standard procedures, adopting an extraction window of 3" centered on the peak of the galaxy's light profile along the slit.

2.2.1. Conversion to the Lick/IDS System

In order to compare measurements of the equivalent widths (EWs) of absorption lines in our observed spectra with model predictions, we need to convert our measurements into the Lick/IDS system. The standard recipe for this calibration has been described in detail by Worthey & Ottaviani (1997). It consists of collecting spectra of Lick/IDS standards (Worthey et al. 1994), smoothing those spectra to the Lick/IDS resolution (given by Worthey & Ottaviani 1997), and comparing the EWs measured in the smoothed spectra with the standard values. In Figure 2 we plot the difference between the EWs of Lick indices measured in our standard star spectra and those measured in the spectra of the same stars in the Jones (1999) spectral library, converted to the Lick/IDS system (for details, see Schiavon 2003, in preparation).

Our measurements are generally in good agreement with the standard values for most of the indices. For some indices we find a systematic trend of the residuals as a function of index strength. The most obvious case is that of Ca4227, but slight trends can also be seen for $H\delta_F$, G4300, Fe4383 and $Mg2$. The errors in our index values were estimated from measurements made on 20 repeat spectra taken for 7 Lick standards. In all cases the errorbars are about the same size as the symbols in Figure 2, indicating that most of the scatter in those plots comes from converting between equivalent-width systems defined by the different instrumental setups. We will henceforth base our errorbars on the *r.m.s.* scatter between our data for Lick standards and the standard values (Figure 2).

A key aspect of such calibrations is that the calibrating standards must encompass the range of EWs characteristic of the target systems, otherwise systematic effects such as that seen in Figure 2 cannot be adequately accounted for, possibly resulting in large errors. For this reason, we indicate by arrows in Figure 2 the index values measured in the spectra of the two targets of our analysis, M67 and M32.

For the indices not exhibiting any slope as a function of index strength, only minor zero point corrections were sufficient to bring our measurements to the Lick/IDS system. That was the case for CN1, CN2, $H\gamma_F$, $H\beta$, Mg b, $Fe5270$, $Fe5335$ and $Mg2$. For the remaining indices, the zeropoint corrections were computed as the average value in a ~ 2

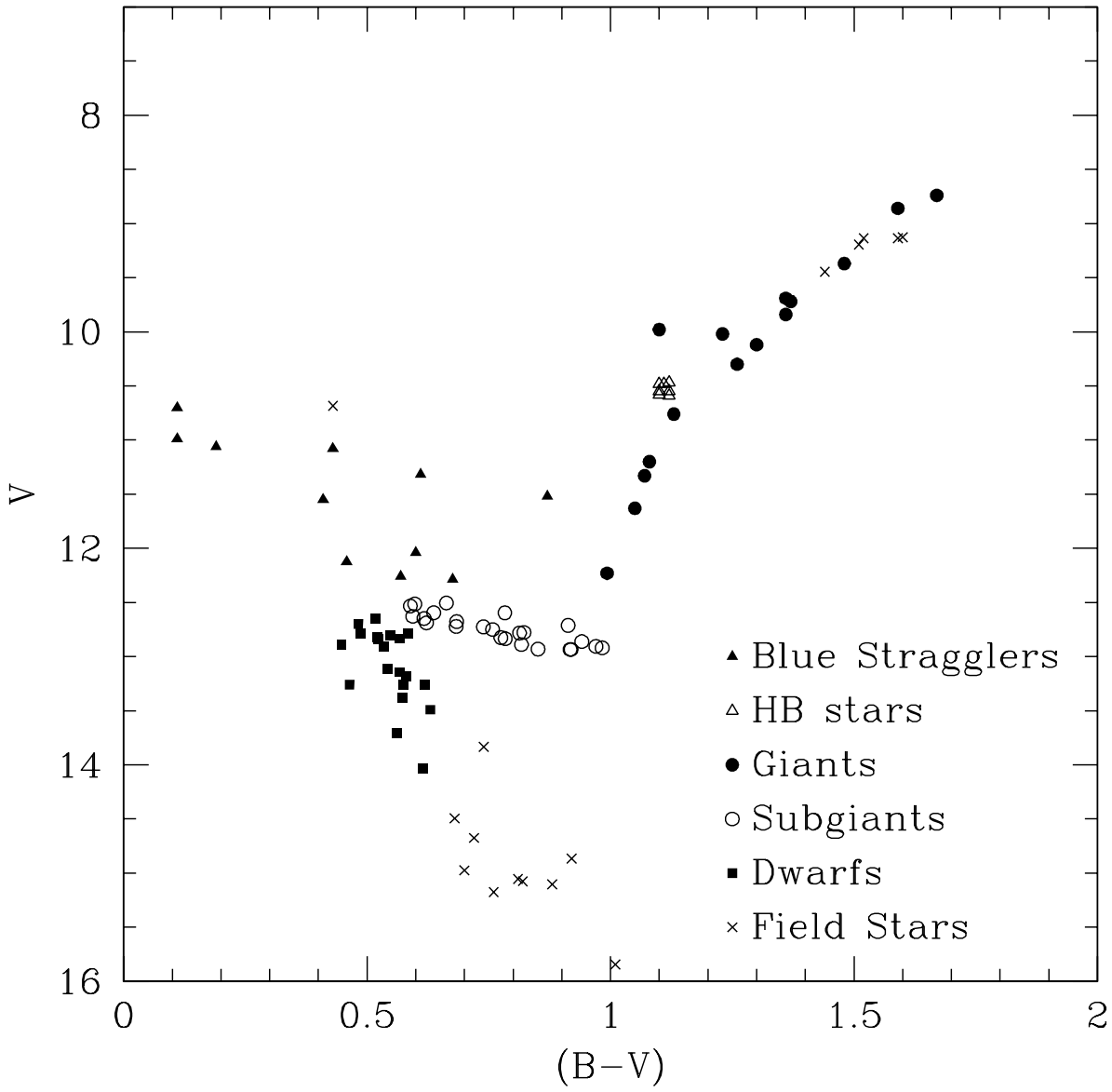

Fig. 1.— Color-magnitude diagram showing the M67 members and field stars observed in this work. The photometry of M67 stars was taken from Montgomery et al. (1993). Our observations of M67 members cover all the evolutionary stages of relevance for integrated light studies in the optical. Different evolutionary stages are denoted by different symbols, indicated in the lower right panel. For completeness, we also observed field stars in areas where the color-magnitude diagram of M67 is scarcely populated (M giants) or where the stars are too faint to be observed efficiently (K dwarfs). Photometry of field stars was taken from the SIMBAD database, together with their Hipparcos parallaxes. The latter data were used to estimate the stars' positions in the CMD as if they were at the distance of M67.

Å-wide window around the values measured for M67 and M32 (0.1 mag in the case of CN1, CN2 and $Mg2$). On average, 15 stars were used in computing the zeropoint corrections. We note that the index values for M67 and M32 are in regions of the index space that are very well populated by standard stars, so that we consider our calibration onto the Lick/IDS system to be robust.

It is important to emphasize how accurately such calibration needs to be done. For instance, a $\pm$0.1Å shift in $H\delta_F$ implies a change in the spectroscopic age of M67 by about $\mp$ 1 Gyr. $H\beta$ and $H\gamma$ are slightly less affected, but the case of the G band (G4300) is especially delicate. There is a sharp decline of the residuals for EWs larger than $\sim$ 5Å, and as a result, if we had adopted a zeropoint correction considering all the calibrating standards, the G4300-based spectroscopic age of M67 would be 2 Gyr older (see discussion in Section 4.2.2).

In Appendix A we provide a table with Lick/IDS index measurements taken in the spectra of all the field and M67 stars observed in this work.

3. The Integrated Spectrum of M67

In this section we describe the construction of the integrated spectrum of M67 from the individual spectra of the stellar members and field stars displayed in Figure 1. The reader who is not interested in technicalities, and would rather focus on the analysis of the integrated spectrum is advised to skip to Section 3.2.

The integrated spectrum of the cluster is given by the following expression

$$F(\lambda) = \sum_{i=1}^{N} f_i(\lambda) \times n_i \times 10^{-0.4(B_i - B'_i)} \quad (1)$$

where $f_i(\lambda)$ is the flux-calibrated spectrum of the *i-th* star and B_i is its B magnitude taken from the Montgomery et al. (1993) photometry. The magnitudes were corrected for interstellar reddening assuming $E(B-V) = 0.05$. B'_i is a magnitude measured in the observed spectrum by integrating it with a B-filter transmittance curve taken from Lejeune, Cuisinier & Buser (1997). The latter step was taken in order to normalize all the spectra in a similar fashion, before weighting them according to the stars' dereddened magnitudes.

The quantity n_i is proportional to the number of stars at each evolutionary stage. For all the stars from the main sequence to the tip of the first-ascent giant branch, n_i was computed assuming a power-law IMF, normalized such that the total mass of the system is equal to

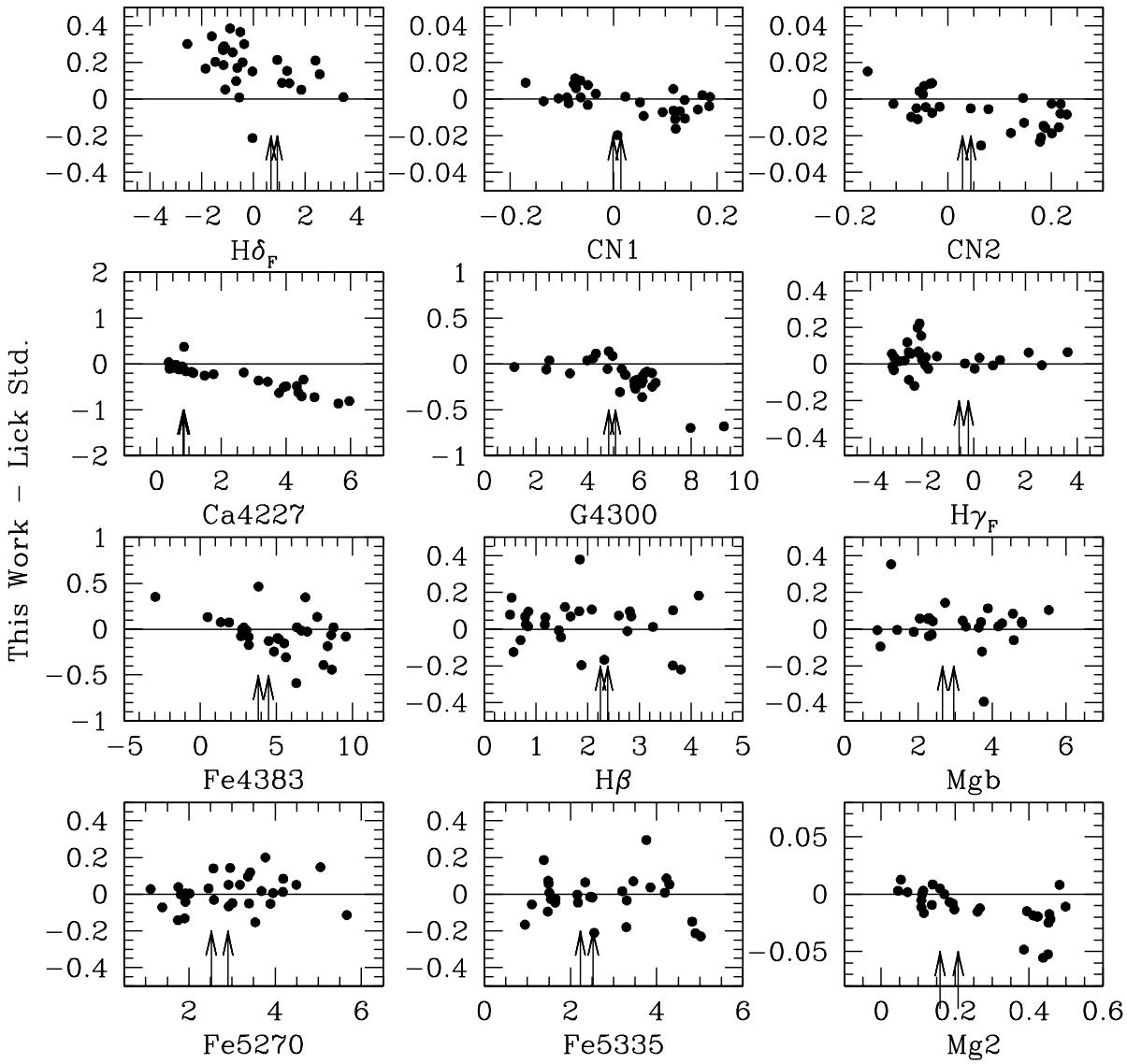

Fig. 2.— Comparison of the line indices measured in our spectra for Lick/IDS standards with the standard values. For all indices (except Ca4227) only minor zeropoint corrections are needed to convert our data to the Lick/IDS system. The arrows indicate the values measured in the integrated spectra of M67 and M32, the main targets of this study, showing that they are in a locus in the index space which is very well populated by standard star measurements. The errobars of our index measurements are about the same size as the symbols.

1 $M_{\odot}$. For horizontal branch stars and blue stragglers, we followed a different procedure as explained a few paragraphs below.

In order to compute n_i, we need to estimate the stellar masses. This was achieved by interpolating stellar colors or magnitudes in a theoretical isochrone for solar metallicity and an age of 4 Gyr. The isochrone was truncated at the tip of the first-ascent giant branch. This procedure was followed for all stars except the M giants ($T_{eff} < 4000$K). The stars are then sorted according to their masses so that the weight for each star was given by

$$n_i = \int_{M_i-(\Delta M_i)/2}^{M_i+(\Delta M_{i+1})/2} M^{-(1+x)} dM \tag{2}$$

where M_i is the mass of the i-th star, x is the IMF exponent, and $\Delta M_i = M_i - M_{i-1}$, so that the mass bin occupied by the i-th star is given by

$$\Delta M = (M_{i+1} - M_{i-1})/2 \tag{3}$$

We adopt a Salpeter IMF, with $x = 1.35$. It can be seen that the weight is higher for lower mass stars, and higher for larger ΔM. The latter means that an individual star in a more densely populated region of the CMD of Figure 1 has a lower weight in the final spectrum because the mass bin occupied by it is narrower. Along the giant branch, the mass varies by just a tiny fraction so that ultimately the weight for each star is mostly dependent on ΔM. This is important for the reasons discussed in Section 3.1

For blue stragglers and horizontal-branch stars, n_i was computed from the observed numbers relative to main sequence stars in the range $14.5 < m_{3890} < 15.5$ as given by the color-magnitude diagrams of Fan et al. (1996) and Deng et al. (1999). This magnitude interval translates into $13.649 < V < 14.427$, according to the color transformations given by equations (3) and (4) of Fan et al.

Fan et al. (1996), analysing photometric data complete down to many magnitudes below the turnoff, found that the present-day mass function of M67 has an exponent $x \sim 0.1$ for masses between 0.8 and 1.2 $M_{\odot}$, and that it levels off for lower masses. They interpret this result as evidence that the cluster has undergone evaporation of low-mass stars. We tested our computations for the effect of the power-law exponent and found that both the overall spectral shape and the absorption line EWs remain virtually constant even for wide variations of x. Therefore, throughout this paper we adopt a single-exponent Salpeter IMF because our interest is in using M67 as a template single stellar population, free of the effects of dynamical evolution.

The assumed value for the reddening towards the cluster has a small impact in the computed integrated spectrum. This effect has been discussed by Schiavon et al. (2002a). It is due to the fact that a variation in $E(B-V)$ implies a change in the inferred absolute magnitudes of the stars, which in turn affect the computed stellar masses, and thus the relative weights given to each star in equation (1). The effect is small, and is indicated in Figures 6 and 7 in the form of arrows.

3.1. Contribution by M Giants to the Integrated Light

For the M giants, the optical colors cannot be used for mass estimation for two reasons: M giants are strongly variable, and optical colors saturate for temperatures below 4000K. The strong variability implies that a given M giant spectrum might not correspond to a measured color if they have not been collected at approximately the same time. On the other hand, saturation makes it difficult to use optical colors to get masses through interpolation in the isochrones. A good example is given by the pair of field stars HD94705 (M5.5III) and HD62721 (K4III). Their $(B-V)$s are 1.46 and 1.53 respectively, but the effective temperatures inferred from the strength of the TiO bands in their spectra are $\sim$ 3400 and 3900 K respectively. If their colors were used to estimate their masses, and thence their weighting factors in equation (1), a large error would result in the case of HD94705, because being cooler it represents a later, less populated evolutionary stage than HD62721.

Our procedure was to estimate the T_{eff}s of all stars redder than $(B-V)=1.3$ from the strength of their TiO bands, using an empirical calibration derived from measurements in the spectra of Lick standards whose T_{eff}s were determined from angular diameter measurements or the infrared flux method (Schiavon 2003, in preparation). The T_{eff}s so derived are listed in Table 4. They were used to estimate stellar masses and colors for stars cooler than $\sim$ 4000K, through interpolation in the theoretical isochrone for 3.5 Gyr and [Fe/H]=0.0. The weights of the M giants resulting from this procedure were substantially higher than when the masses were interpolated from their $(B-V)$s, because there are only four M giants in our sample, and therefore each of these stars occupies a wide mass bin (equations 2 and 3). As a result, when the M giants are accounted in this way, the strength of the redder indices, especially Mg b, becomes considerably stronger. In fact, the latter index becomes $\sim$ 0.3 Å stronger than when the masses of M giants were (wrongly) estimated from their colors. $H\beta$ is also affected, but to a lesser degree.

The dependence of Mg b and $H\beta$ on the contribution by M giants is due to the very strong TiO bands present in their spectra, which can sizeably affect the redder Lick indices. To illustrate this, we compare in Figure 3 the spectra of HD62721 and HD94705, overlaid

by horizontal lines indicating the passband and pseudocontinuum definitions of $H\beta$ and Mg b. As can be seen, strong TiO bandheads coincide with the index passbands. In particular, in the case of Mg b, the M giant spectrum is roughly 6 times brighter in the blue pseudo-continuum window than in the index passband. Therefore, increasing the contribution by M giants to the integrated light causes a substantial increase in Mg b. As a consequence, it is very important to compute the weights of the M giants precisely, because even though their contribution to the total integrated light in the optical is not very large, their influence on key spectral indices like Mg b and $H\beta$ is by no means negligible. It goes without saying that SP model predictions for such indices are likewise afflicted by such uncertainties. This is an issue that is seldom appreciated in the literature, in particular by stellar population modellers. The situation is of course even more serious for indices located towards the far red where the contribution of M giants to the integrated light is dominant (e.g. Schiavon, Barbuy & Bruzual 2000, Schiavon & Barbuy 1999).

Another important issue regards the luminosity function in the upper giant branch. In particular, our procedure to compute the integrated spectrum of M67 needs to account for stars in the asymptotic giant branch (AGB). Recall that when we computed the weights for the stars in equation (1), we truncated the isochrone used in the computation of stellar masses at the tip of the first-ascent giant branch. In order to account for the AGB stars, we increase n_i for stars brighter than the horizontal branch by 0.1 dex, according to the theoretical LF of the Padova isochrones.

3.2. Resulting Integrated Spectrum and the Effect of Blue Stragglers

The resulting integrated spectrum of M67 is displayed in Figure 4, where we compare the spectra obtained with and without the contribution by blue stragglers (BS). As can be seen in this figure, the contribution to the integrated light due to BS is very large: when BS are included in the computation, the resulting spectrum is considerably bluer and has stronger Balmer lines and weaker metal lines. This result agrees with the finding by Deng et al. (1999), who modelled the cluster's integrated light using intermediate band photometry and synthetic stellar spectra from the Kurucz spectral library. Landsman et al. (1998) assessed the relative contribution of BS stars to the integrated light of M67 in the ultraviolet and found that BS dominate the light of the cluster at ~ 1500Å. It is important to stress that this result does not depend on any assumption as to the number ratio of BS to main sequence stars, as the latter number is anchored on photometry and membership studies. Recall that our recipe to weigh BS in number is based on the photometry by Fan et al., which is complete down to many magnitudes below the turnoff.

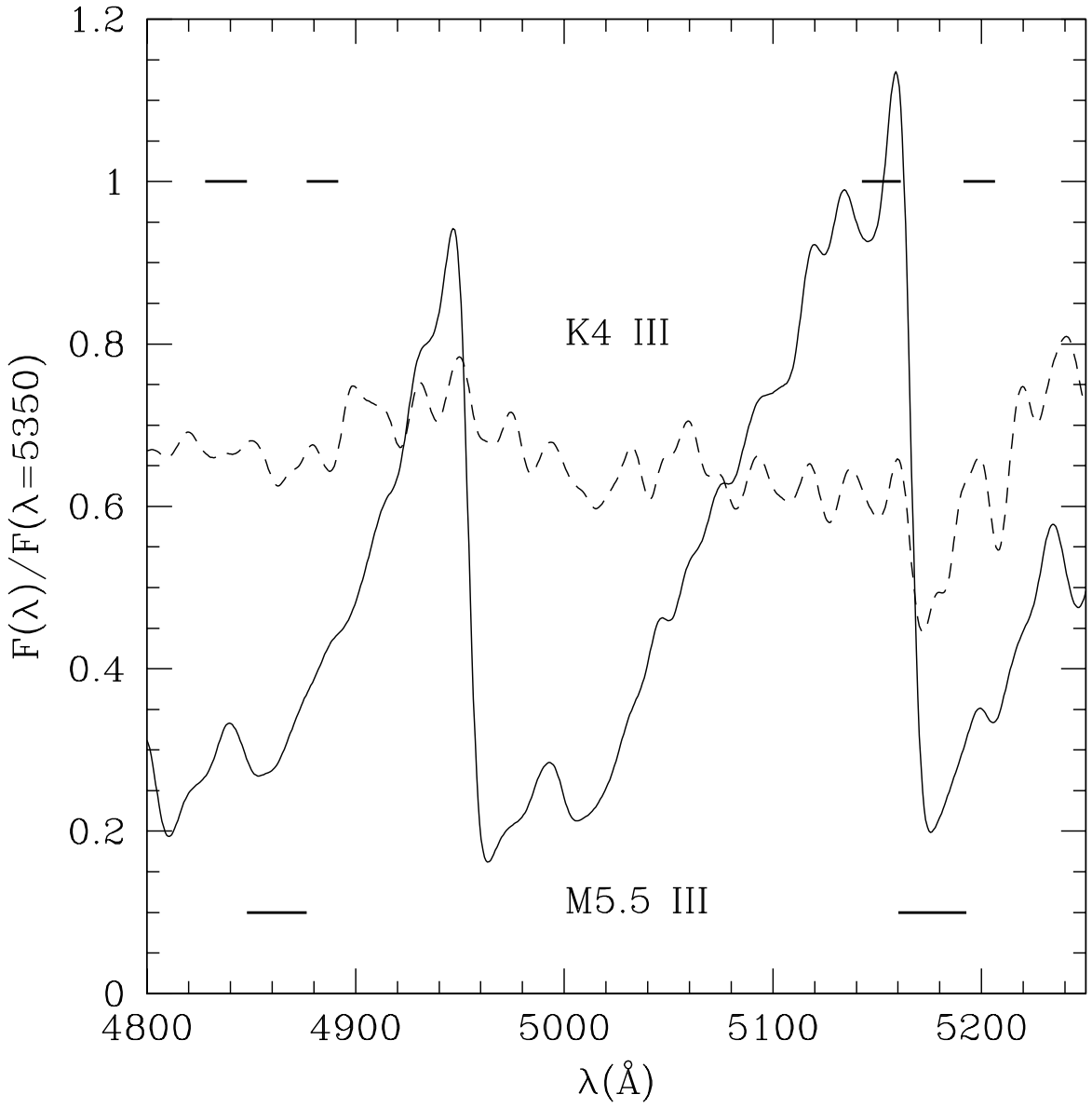

Fig. 3.— Comparison between the spectra of two giants: HD94705 (M5.5III, solid line) and HD62721 (K4III, dashed line), with essentially identical $(B-V)$s. The pseudocontinua and passband of $H\beta$ (left) and Mg b (right) are illustrated by the horizontal lines. The spectrum of the M giant is characterized by very strong TiO bands, whose bandheads coincide with the passbands and continuum windows of the Lick indices. The case of Mg b is particularly sensitive, since M giant stars contribute roughly 6 times more flux in the blue pseudocontinuum than in the index passband. For this reason, errors in estimating the contribution of very cool stars to the integrated light of M67 can cause sizeable errors in the integrated value of Mg b. The same comments apply, to a lesser extent, to $H\beta$.

The BS frequency in M67 appears to be unusually high when compared with other clusters of similar age and richness (e.g., Ahumada & Lapasset 1995, see also a discussion in Landsman et al. 1998). Hurley et al. (2001), using binary population synthesis and N-body simulations, propose that the high BS fraction in M67 is due to a combination of effects related to binary evolution, stellar encounters in the cluster high density environment, and evaporation of low-mass stars.

Irrespective of the physical origin of the BS phenomenon, their mere existence is a potential source of confusion for those attempting to use Balmer lines to date stellar populations, as is clearly illustrated by the strength of Balmer lines when BS are included in the integrated spectrum (Figure 4). In fact, we show in Section 4.2 that the age one would infer from the integrated spectrum of M67 when blue stragglers are included is substantially lower ($\sim$ 1.2 Gyr). However, the case of M67 seems to be exceedingly unusual. As noted by Landsman et al. (1998), the central stellar density in the cluster is higher than that found in the centers of most nearby galaxies.

There is another reason to believe that such a high BS contribution does not seem to be a common phenomenon in the Universe, and in particular in early-type galaxies, which are the ultimate targets of our modelling efforts. When blue stragglers are included, the integrated spectrum of M67 has strong enough Balmer lines that it would be classified as a *k+a/a+k* spectrum according to the definition of several different groups (Fisher et al. 1998, Balogh et al. 1999, Tran et al. 2003, Poggianti et al. 2003). Therefore, it is reasonable to assume that such a high fraction of blue stragglers as found in M67, if common to the centers of early-type galaxies, would generate a high fraction of *k+a/a+k* galaxies in the Universe. However, recent estimates from the Sloan Digital Sky Survey rate the fraction of *k+a/a+k* galaxies in the local Universe at slightly lower than 0.1% (Goto et al. 2003). We therefore conclude that a blue-straggler population as seen in M67 is, at most, extremely rare in field galaxies, and henceforth concentrate on comparing our models with the integrated spectrum of M67 without the contribution of blue stragglers. This is the topic of the next section.

The spectra shown in Figure 4 are helpful templates for the calibration of stellar population models, in an age/metallicity regime where these models still remain largely untested. Therefore, we make them available electronically upon request to the authors.

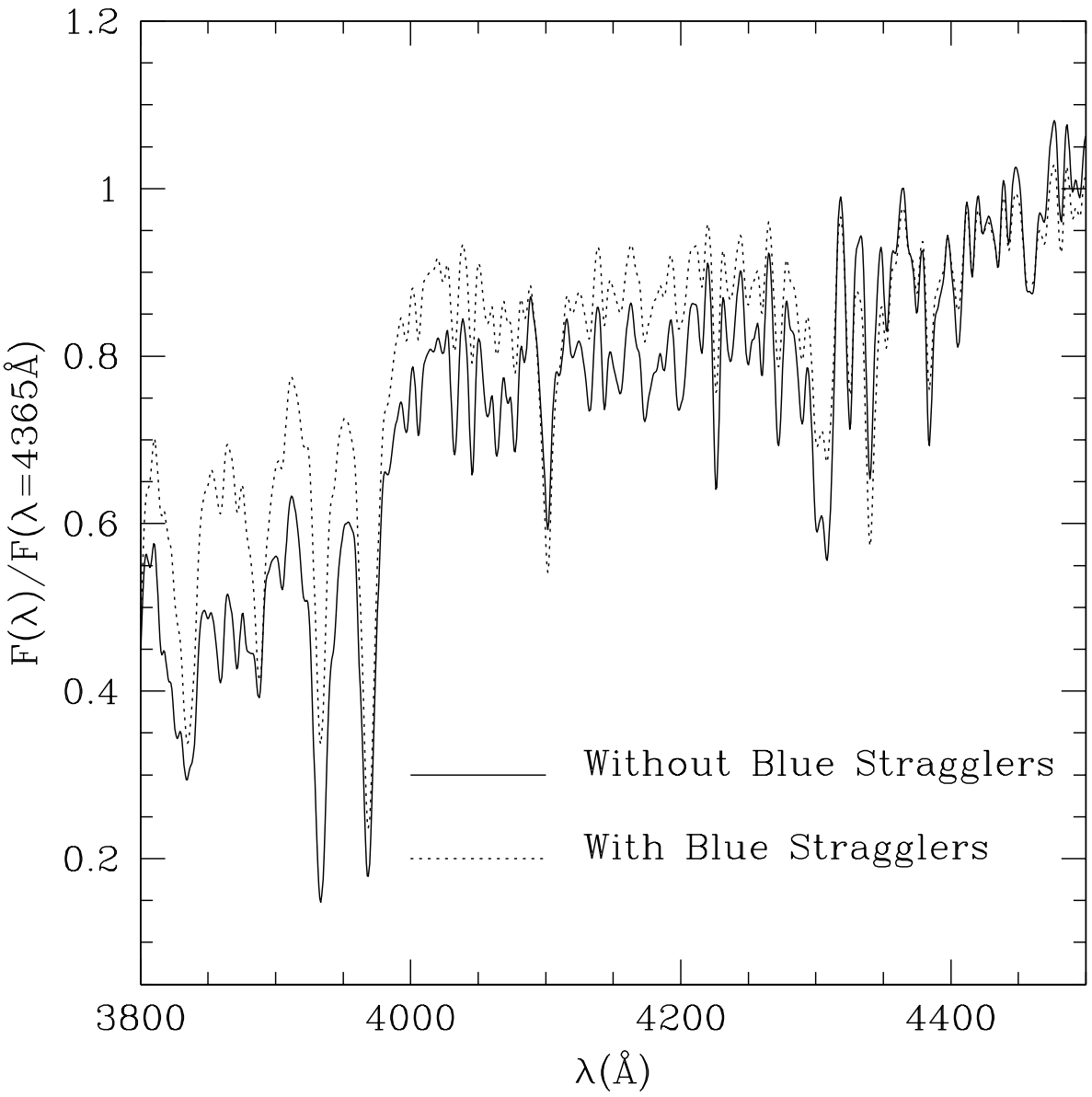

Fig. 4.— Integrated spectrum of M67, resulting from the computations described in Section 3. The spectrum represented by the solid line was obtained without considering the contribution due to the blue stragglers. The spectrum obtained when the latter are included is shown as the dotted line. The contribution due to the blue stragglers is very large. This is a robust result, since the number of blue stragglers relative to main sequence stars is solidly constrained by photometry and membership studies.

4. Comparing Stellar Population Models with the Data for M67

4.1. The Turn-off Age of M67

In this section we estimate the age of M67 from the comparison of its color-magnitude diagram with theoretical isochrones. This is a very important step, as in the next section we will require our SP computations to be consistent with the ages inferred from the CMD, using the *same* set of isochrones in both procedures.

The iron abundance of M67 is about or slightly below solar (Brown 1987, Hobbs & Thorburn 1991, Friel & Boesgaard 1992, Tautvaisiene et al. 2000, Shetrone & Sandquist 2000), and the abundance ratio between α-elements and iron also seems to be nearly solar (Friel & Boesgaard 1992, Shetrone & Sandquist 2000, Tautvaisiene et al. 2000). Therefore we adopt the isochrones by Girardi et al. (2000) for solar metallicity. Girardi et al.'s isochrones are computed for the solar mixture of heavy elements, and we will henceforth refer to them as the Padova isochrones.

In Figure 5 we display the color-magnitude data for M67 from Montgomery et al. (1993), overplotted on the Padova isochrones for solar metallicity and ages of 2.8, 3.5 and 4.4 Gyr. The isochrones were transformed to the observational plane adopting the color vs. T_{eff} calibration described in Schiavon et al. (2002a) and the bolometric correction vs T_{eff} calibration from Alonso et al. (1995,1999).

The reddening determinations for M67 range from $E(B-V) = 0.03$ (Fan et al. 1996, Nissen, Twarog & Crawford 1987) to 0.05 (Montgomery et al. 1993, Taylor 1980). We adopted a reddening of $E(B-V) = 0.05$, within the range of previous determinations. The distance modulus adopted was $(m-M)_0$=9.45 (Chaboyer et al. 1999). The age error due to the uncertainty in the reddening towards the cluster is very small, mostly because at ages around 3-4 Gyr the color and luminosity of the turnoff are very age-sensitive – as opposed to what happens for older ages (see discussion in Schiavon et al. 2002b). However, the uncertainties on the distance modulus and reddening do have some impact on the final integrated spectrum, as discussed in Section 3.

Deciding the exact position of the cluster's turnoff in Figure 5 is not obvious. There is a sparse group of stars between $V \sim 12.5$ and ~ 12.0 at $(B-V) \sim 0.6$ that seems to be well fitted by the "hook" above the turnoff of the 2.8 Gyr isochrone. If these stars are not considered to be blue stragglers, then the best-fitting cluster age would be ~ 2.8 Gyr. Conversely, if the "hook" is considered to be the clump of stars at $V \sim 12.7$ and $(B-V) \sim 0.6$, the 3.5 Gyr isochrone would be a better fit. For consistency, we adopt the older age as the best fit, because the stars brighter than $V \sim 12.5$ were considered to be

blue stragglers when we computed the integrated spectrum of the cluster (see Figure 1). Therefore, for our present purposes, we adopt an age of 3.5 Gyr for M67. We note that Chaboyer, Green & Liebert (1999), analysing the same photometric data, adopted a similar criterion to define the cluster turnoff, and find the same age for the cluster, even though they adopted a different set of isochrones and a different distance modulus. Most importantly, our age and distance modulus estimates are within the range of previous results in the literature: age = 3.5 – 5 Gyr, $(m-M)_0 = 9.35$ – 9.60 mag (see the review by Chaboyer et al. 1999 for details).

The assumption of convective core overshooting can also potentially affect age determinations in the intermediate age regime ($\lesssim$ 4 Gyr), where turn-off stars have masses $m \gtrsim 1.5 M_{\odot}$ (e.g. Maeder & Meynet 1991). The isochrones by Girardi et al. (2000) include mild overshooting for stars with $m > 1.5 M_{\odot}$ and a gradual decrease of the overshoot efficiency with decreasing mass down to $m = 1 M_{\odot}$, where overshooting is turned off. The best-fitting isochrone in Figure 5 has a turn-off mass of $\sim 1.4 M_{\odot}$, which is within the regime of low overshooting efficiency in the Girardi et al. isochrones. Therefore, the age derived here should not be significantly dependent on the model prescription for overshooting.

Finally we would like to stress that, for the purposes of this paper, it is not crucial to determine the absolute age of M67. Much more important for us is to focus on reaching consistency between spectroscopic and CMD-based ages. This is the topic of the next section.

4.2. Comparison with Stellar Population Models

4.2.1. The Models

Before discussing the estimation of the age and metal abundances of M67 from its integrated spectrum, we recapitulate our modelling techniques.

The key ingredients of our models are a set of theoretical isochrones from the literature, a set of calibrations used to transform the latter into the observational plane, and a set of fitting functions, which are used to compute absorption line indices as a function of stellar parameters. The latter are integrated along the isochrones in order to produce integrated line indices of single stellar populations. The isochrones adopted here are the ones by Girardi et al. (2000), which were already presented in Section 4.1. The calibrations used to transform T_{eff} and M_{bol} into colors and magnitudes are a combination of those presented in Schiavon et al. (2002a) and the empirical calibrations by Alonso et al. (1995,1999).

The fitting functions are the major new ingredient of our models. They are based on

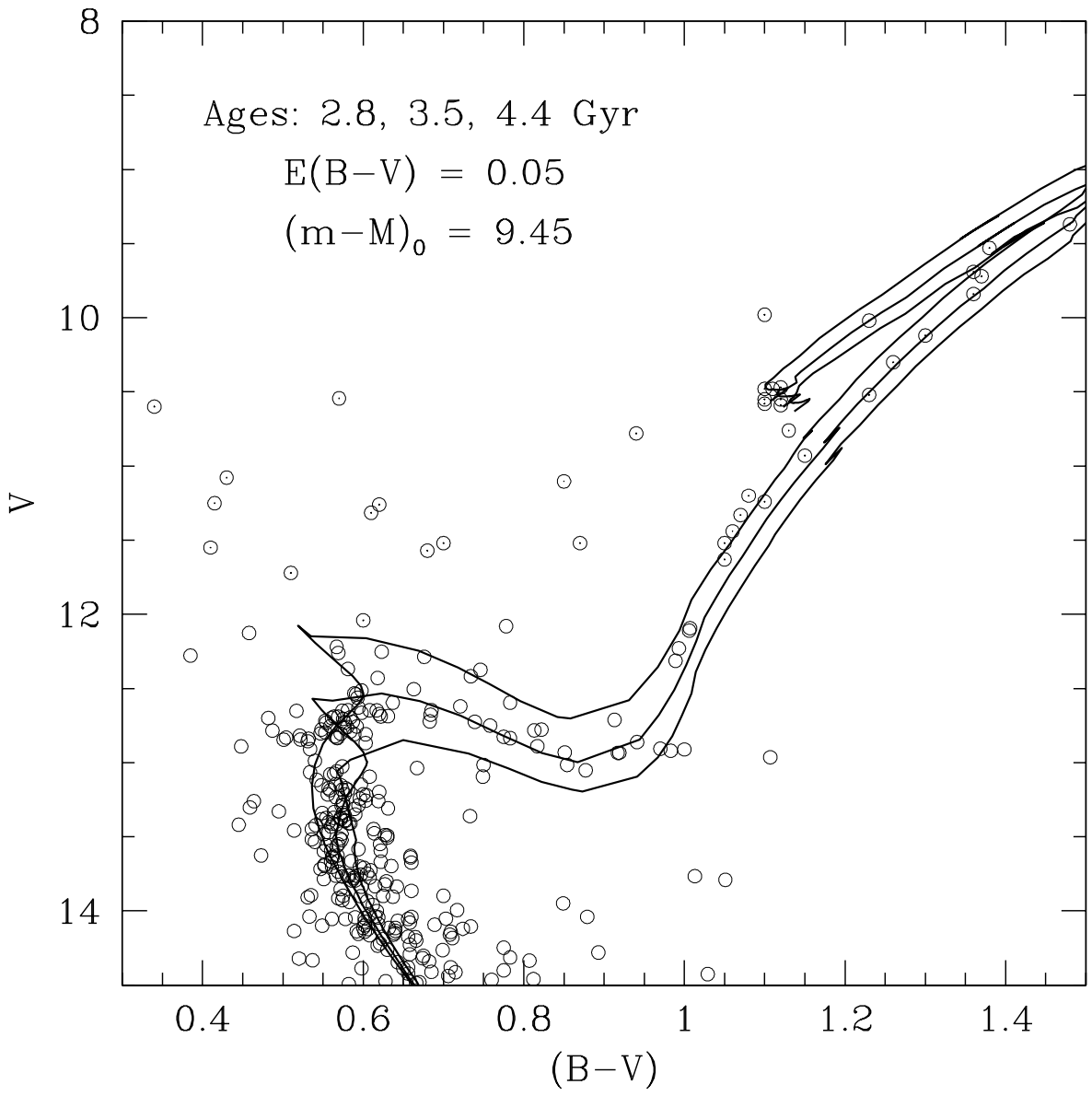

Fig. 5.— Comparison between the color-magnitude diagram of M67 (data from Montgomery et al. 1993) and the isochrones from Girardi et al. (2000). The isochrones were transformed to the observational plane using the recipe described by Schiavon et al. (2002a) and the reddening and distance modulus indicated in the top left. From left to right, the ages of the theoretical isochrones are 2.8, 3.5 and 4.4 Gyr. The age that best fits the cluster data is 3.5 Gyr.

a redefinition of the Lick/IDS system, rooted in the Jones (1999) spectral library (a brief description can be found in Jones & Worthey 1995), converted to the Lick/IDS resolution, and supplemented by further data from the original Lick/IDS library (Worthey et al. 1994). Most importantly, the fitting functions are based on a new set of homogeneous stellar parameters for the stars from the Jones spectral library. A detailed description of our stellar parameter determinations can be found in Schiavon et al. (2002a). A full description of the models, including a thorough comparison of our new fitting functions with those from the literature, will be presented elsewhere (Schiavon 2003, in preparation).

4.2.2. The Spectroscopic Age of M67 According to the SP Models

The absorption line indices measured in the integrated spectrum of M67 are listed in Table 5 and compared with the predictions of single stellar population models in Figures 6 and 7. The 1-σ errorbars listed in Table 5 and adopted in all the figures involving integrated indices were estimated from the *r.m.s.* scatter between our measurements of Lick indices in Lick/IDS standard stars and the standard values (see Figure 2). Assuming equal contribution to the *r.m.s.* scatter from our measurements and the standard values, we divide the *r.m.s.* by $\sqrt{2}$ to obtain the error estimates. These errors are certainly larger than expected from Poisson statistics and wavelength calibration errors, and so they are dominated by systematic effects of tying into the Lick/IDS system with spectra taken from different sources. Since the M32 and M67 composite spectra have very high S/N ratio, comparable to those of the standard stars, we assume the same overall errors for M32 and M67.

We choose to compare the models with the observations using four age indicators ($H\delta_F$, G4300, $H\gamma_F$ and $H\beta$) and five metal abundance indicators (CN1, CN2, Fe4383, $< Fe >$ and Mg b). Index definitions can be found in Worthey et al. (1994) and Worthey & Ottaviani (1997). In the figures, dotted lines connect models with the same age, and solid lines connect models with the same metallicity. The ages plotted are, from top to bottom, 1.2, 2.0, 2.5, 3.5, 7.9 and 14.1 Gyr, and the metallicities are, from right to left, [Fe/H] = +0.2, 0.0, –0.4, –0.7 and –1.3 (the latter two are absent in some plots, for clarity). The lines connecting models with [Fe/H]=0 and with t = 3.5 Gyr are thicker. Indices measured in the spectra of M67 with and without blue stragglers are represented by the open square and circle, respectively.

The most striking feature in these figures is that all Balmer lines indicate the same age for M67, within less than 1 Gyr. Moreover, the spectroscopic age according to the Balmer lines is $\sim$ 3.5 Gyr, in agreement with that inferred in Section 4.1, from the comparison of cluster data with theoretical isochrones in the color-magnitude diagram. We highlight the fact that the *same* isochrones were employed in deriving the spectroscopic and CMD

ages. Even though such consistency should in principle be expected, we note that previous studies found huge discrepancies between CMD-based and spectroscopic ages for a well-known Galactic globular cluster, 47 Tuc. The turnoff age of this cluster is 11 ± 1 Gyr when the isochrones of Salaris and collaborators (see description in Vazdekis et al. 2001) are employed. However, Gibson et al. (1999) found a spectroscopic age in excess of 20 Gyr for the cluster. Later on, Vazdekis et al. (2001) showed that better agreement was reached when effects like α-enhancement and diffusion of heavy elements are taken into account. However, a mismatch of 4 Gyr was still lingering. Schiavon et al. (2002b) finally showed that most of the discrepancy was due to a mismatch between the theoretical luminosity function of the brighter giant stars and the observations, in the sense that theory predicted too few bright giants. Therefore, considering the previous history, it is quite reassuring that our single stellar population models provide results at this level of consistency, in a regime where SP models have never been tested before in such a level of detail.

The remaining age indicator, the G band (G4300) presents a trend as a function of age which is opposite to that of Balmer lines: it gets weaker for younger ages. This is due to the fact that it is much stronger in giants than in turnoff stars. As a result, the G band gets stronger in the integrated spectra of older stellar populations because they are characterized by a higher relative contribution of giant stars to the integrated light. Being mostly due to the CH molecule, the G band is not expected to be a clean age indicator, due to its dependence on the abundance of carbon. In fact, we obtain an older age for M67 from the EW of the G band ($\sim$ 6 Gyr). Tripicco & Bell (1995) showed that the G band is mostly sensitive to the abundance of carbon. According to their calculations, the mismatch between the model for [Fe/H]=0.0 and age = 3.5 Gyr is such that it could be explained by M67 having a higher than solar [C/Fe]. However, abundance studies of M67 turnoff stars point at a different direction: they have nearly solar [C/Fe], and may even perhaps be a little carbon-poor (see discussion in Section 4.2.3).

Therefore, it is quite puzzling that in the M67 integrated spectrum the G band is stronger than in the model for 3.5 Gyr and solar metallicity. We tried removing stars very deviant from the average relation between the EW of the G band and color, but that did not remove the discrepancy. We showed in Section 2.2.1 that the calibration of our G band measurements into the Lick/IDS system was somewhat uncertain. We thus believe that calibration uncertainties related to the conversion into the Lick/IDS equivalent width system are responsible for this mismatch.

In Section 3.1, we corrected our model predictions for the effect of AGB stars, by adding an extra 0.1 dex in the luminosity function of the upper giant branch. In their analysis of the integrated spectrum of 47 Tuc, Schiavon et al. (2002b) showed that an error of ± 0.1 dex in

the luminosity function of giants brighter than the horizontal branch translates into an error of ± 1 Gyr in the spectroscopic age inferred from Balmer lines. The latter result is valid for an old stellar population (∼ 11 Gyr) with [Fe/H]=–0.7. For a younger and more metal-rich stellar population, we expect the effect to be less important, given that the total contribution by cool giants to the optical integrated light of metal-rich SPs with intermediate ages is lower. In fact, we note that the integrated spectrum of M67 is little affected by uncertaintities in the LF of the upper giant branch: the change in the M67 indices in Figures 6 and 7 that would be generated by a 0.1 dex variation in the LF above the horizontal branch is in all cases smaller than the symbol size.

In summary, we achieve excellent consistency for M67 between the spectroscopic ages inferred from all Balmer lines studied. We attribute the mismatch with the spectroscopic age inferred from the G band to uncertainties in the calibration of the latter.

4.2.3. The Metal Abundances of M67 According to the SP Models

Figures 6 and 7 also allow checking the consistency of SP model predictions with the known elemental abundances of M67. This is a unique opportunity, because M67 stars have been the subject of many abundance analyses by different groups, so that it can be fairly said that the abundance pattern of the cluster is well known. The importance of enforcing consistency between SP models and the results of classical stellar abundance analyses lies in the fact that the latter provide the only physically meaningful measurement of the abundances of heavy elements in stars. We emphasize that such a tight consistency is seldom attempted in the literature. A similar approach was followed in our study of the mildly metal-rich Galactic globular cluster, 47 Tuc (Schiavon et al. 2002a,b), and now we provide, for the first time, a check of the consistency of SP models in the regime of intermediate age and solar metallicity. For this purpose, we below discuss separately a few relevant elements, together with a brief summary of the previous results from detailed abundance analysis of M67 stars.

Iron

Classical abundance analysis of M67 members, based on high-dispersion spectroscopy, was pioneered by Cohen (1980), who found <[Fe/H]> = –0.39, from a study of four cluster giants. This result was revised by subsequent studies which found a higher iron abundance, near the solar value. Foy & Proust (1981), analysing two giant stars, found <[Fe/H]> –0.1 ± 0.1. Garcia Lopez, Rebolo & Beckman (1988), who studied seven turnoff and one giant

star found <[Fe/H]> = +0.04 ± 0.04. Friel & Boesgaard (1992) analysed three cluster dwarfs and found <[Fe/H]> = +0.02 ± 0.1. Most recently, Tautvaisiene et al. (2000) found <[Fe/H]> = –0.03 ± 0.15, in an analysis of nine giant stars, and Shetrone and Sandquist (2000) determined <[Fe/H]> = –0.05 ± 0.05 for four turnoff stars. In view of these previous studies, we assume that M67 has a solar iron abundance (<[Fe/H]> = 0 ± 0.1).

The line indices in Figures 6 and 7 that are most sensitive to the iron abundance are $< Fe >$ and Fe4383 Figures 6 and 7 indicate that both indices are consistent with <[Fe/H]> = 0 to within less than 0.1 dex.

Carbon and Nitrogen

The abundances of these elements are very important because they affect significantly the indices blueward of 4500 Å, due to the presence of thousands of CN and CH lines (for a discussion, see Schiavon et al. 2002a). The abundance of carbon also has an important effect on Mg b, due to contamination by C_2 lines (Tripicco & Bell 1995). Brown (1987), analysing stars at different evolutionary stages, found that the C/N abundance ratio in M67 stars undergoes a sharp drop between $M_V \sim 3.5$ and ~ 2.8, as a result of the first dredge-up episode. Subsequent analyses are consistent with this result. Regarding carbon, analyses of dwarf stars by Friel & Boesgaard (1992) and Shetrone & Sandquist found <[C/Fe]> = –0.1 ± 0.2 and 0.0 ± 0.1, respectively, while Tautvaisiene et al. (2000), analysing giant stars, found <[C/Fe]> = –0.2. Nitrogen abundances are more uncertain, and also there are fewer determinations in the literature. Tautvaisiene et al. found that M67 giants have <[N/Fe]> = +0.2, whereas Shetrone & Sandquist, analysing turnoff stars, found <[N/Fe]> = +0.1 ± 0.2. In summary, [C/N] is $\sim$ 0.25 dex lower in M67 giants than in dwarfs. In particular, we emphasize that the abundance ratios in M67 giants are nonsolar, whereas M67 dwarfs are consistent with a solar carbon abundance, while perhaps being slighty enhanced in nitrogen.

In Figure 6, it can be seen that our model prediction for 3.5 Gyr and [Fe/H] = 0 is in excelent agreement with the measurements of the CN indices in the integrated spectrum of M67, even though our models have, nominally, solar abundance ratios. This can be understood in view of the results of Gratton et al. (2000) and Carretta, Gratton & Sneden (2000), who showed that in field stars the first dredge-up operates a change in the surface composition of carbon and nitrogen which is very similar to what is seen in M67 and other clusters. Therefore, in the field stars that serve as the basis of our models, the run of C,N abundances as a function of evolutionary stage is arguably similar to that of M67 stars, so that the effects due to stellar evolution in M67 stars are accounted for in the models by construction (this has first been pointed out by Gorgas et al. 1993). Therefore, no correction due to nonsolar abundance ratios needs to be applied to our model predictions and M67 stars

can be considered to constitute a single stellar population with solar [C,N/Fe].

Magnesium

The index in Figure 7 which is most sensitive to the abundance of magnesium is Mg b, which is the most popular estimator of the metallicities of stellar populations of galaxies, and therefore it is very important that our predictions be consistent with the abundance analyses of M67 stars for magnesium. There is some disagreement in the literature as to the magnesium abundance of M67. Foy & Proust found <[Mg/Fe]> = 0, Tautvaisiene et al. (2000) found <[Mg/Fe]> = +0.1, and Shetrone & Sandquist found <[Mg/Fe]> = –0.1. In Figure 7, it can be seen that our model prediction for Mg b is somewhere between [Mg/Fe] = –0.1 and 0.0, and so it is consistent with abundance analysis work. However, we stress that more work is needed in order to ascertain the magnesium abundance of M67.

In summary, we conclude that our model predictions are consistent to within ± 0.1 dex with the known metal abundances of M67. This is reassuring, because it implies that our models predict the correct values of abundance-sensitive indices which are among the most widely used in stellar population work. We also emphasize that the predictions are consistent for indices which are sensitive to the abundances of a number of important chemical species, like iron and the light elements carbon and nitrogen, and magnesium. This also means that the models can be used to estimate luminosity-weighted abundance ratios of galaxies in a way that is consistent with the state of the art of our knowledge of stellar abundances in the Galaxy.

5. The Spectroscopic Age and Metal Abundances of M32

We would like to start our discussion of the SP properties of M32 by reminding the reader that our spectrum is integrated within a square 3" on a side positioned on the center of the galaxy. This is important in view of the fact that previous studies have indicated the presence of a radial gradient in the spectroscopic properties of M32 (Davidge 1991, González 1993, Hardy et al. 1994, Worthey 2003).

Because of its morphology, proximity, and very high central surface brightness, M32 has become a benchmark for the study of stellar populations, and galaxy evolution in general. Spinrad & Taylor (1971), and Faber (1973) pioneered the efforts to determine the

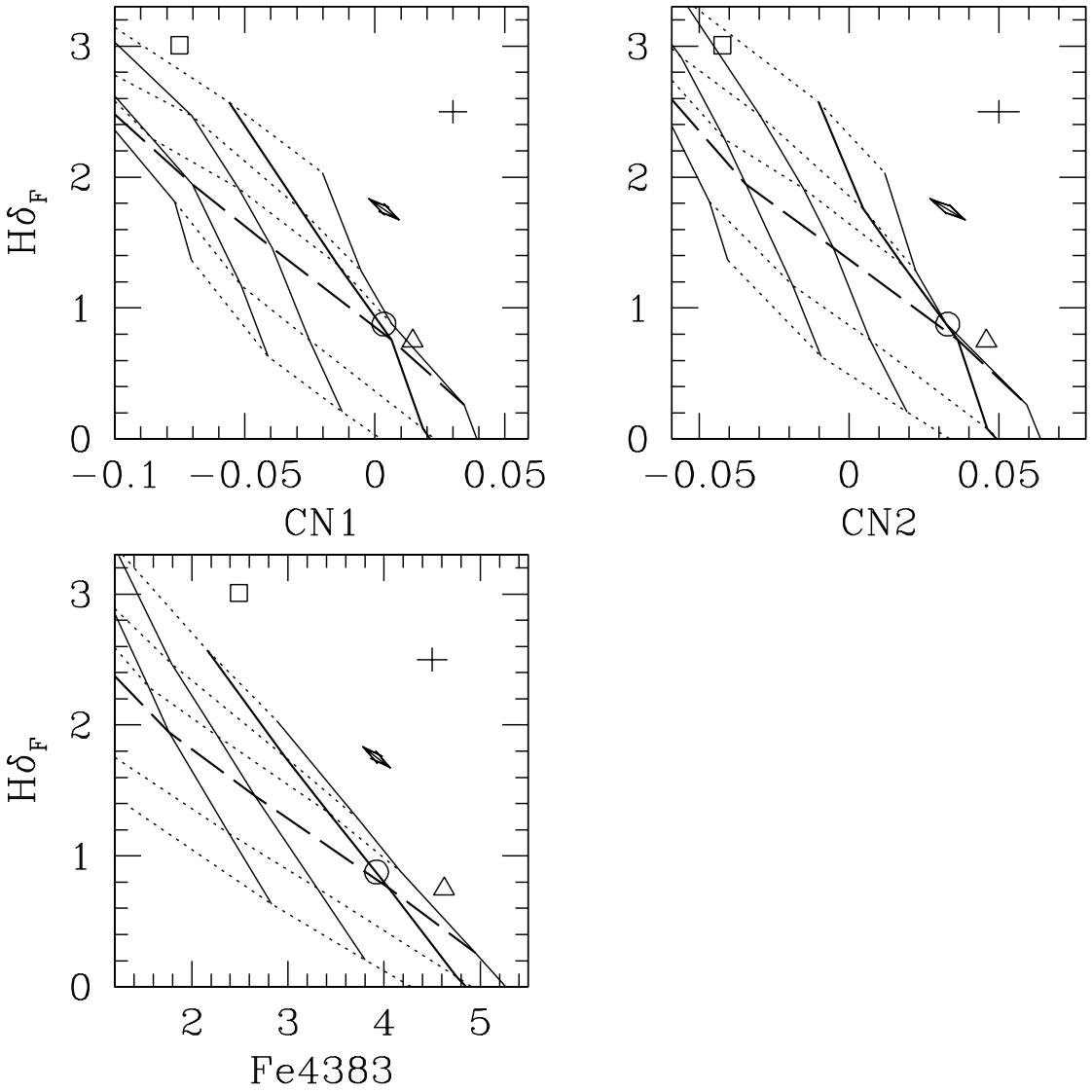

Fig. 6.— Comparison of model predictions absorption line indices for single stellar populations with those measured in the spectra of M32 (open triangle), M67 without blue stragglers (open circle) and M67 including blue stragglers (open square) Dotted lines connect model predictions for the same age. From top to bottom: 1.2 2.0, 2.5, 3.5, 7.9, and 14.1 Gyr. Solid lines connect model predictions for the same [Fe/H]. From right to left: +0.2, 0.0, –0.4, –0.7, and –1.3 (in some c, the line for [Fe/H]=–1.3 falls outside the plotting area). The lines for [Fe/H]=0.0 and age=3.5 Gyr are thicker, for clarity. The arrows indicate by how much the integrated indices of M67 vary for an error of ± 0.015 in $E(B-V)$. A higher reddening makes Balmer lines look stronger and metal lines weaker. The spectroscopic age of M67, when blue stragglers are not included in the integrates spectrum, is about 3.5 Gyr in all diagrams, which is in agreement with the value inferred from the CMD. The data on M32 indicate that it has super-solar iron abundance and has a nearly solar abundance of carbon and/or nitrogen, relative to iron.

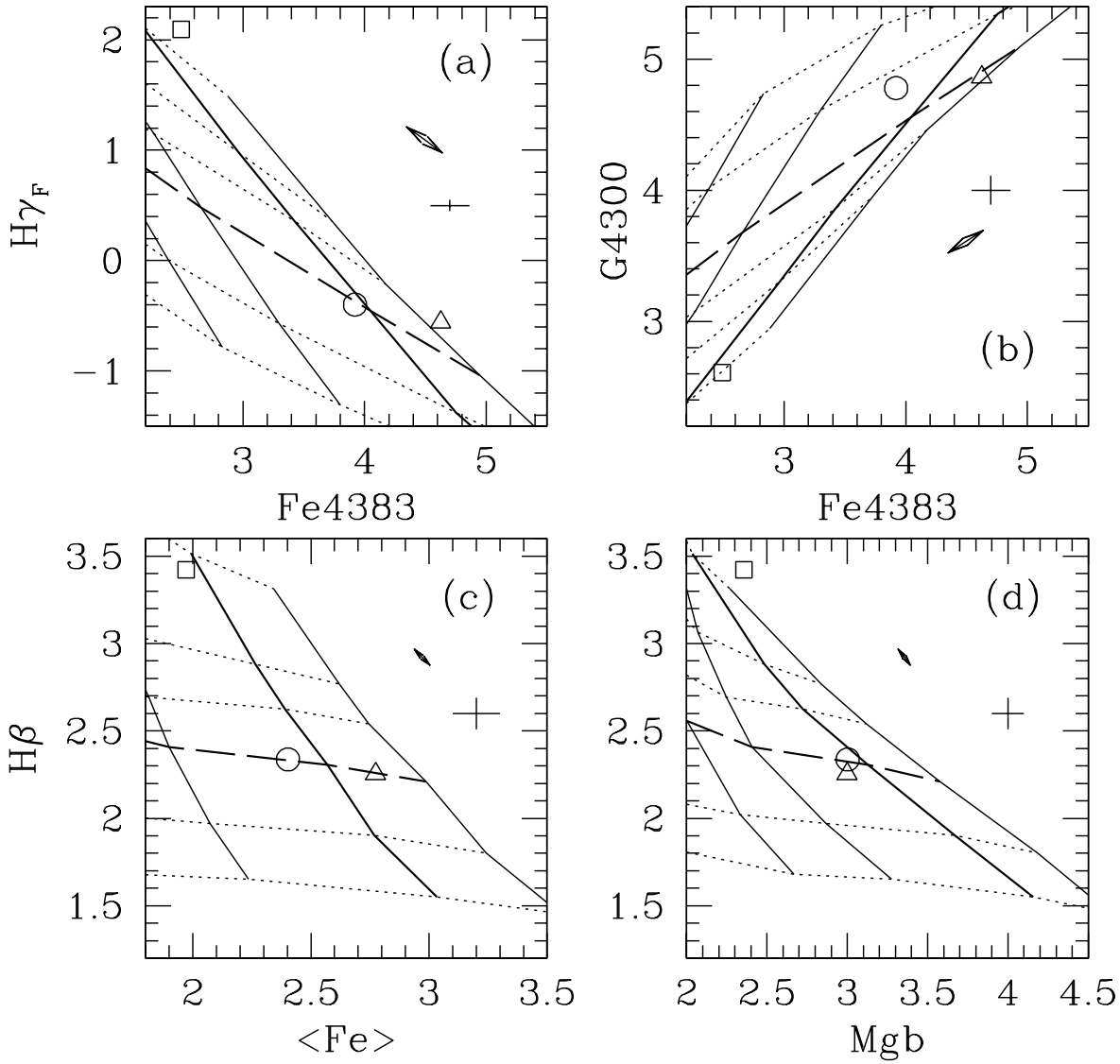

Fig. 7.— Same as Figure 6. Symbols are the same as for Figure 6. The most important conclusions to be drawn from this figure and Figure 6 are: 1) All Balmer lines indicate the same age for M67, in agreement with the CMD-based age; 2) The Fe, CN and Mg indices indicate solar abundances within ± 0.1 dex, in agreement with spectroscopic studies of stellar members. 3) When blue stragglers are included in the integrated spectrum of M67, the spectroscopic age drops to ∼ 1.2 Gyr, or even younger, depending on the line index adopted. For the G band the dependence on age is inverted, so that age decreases from top (14.1 Gyr) to bottom (2.0 Gyr). Ages based on the G band, are too old (a factor of two in the case of M67). For M32, bluer Balmer lines tend to indicate younger ages, and bluer Fe lines indicate higher metallicities. The data on M32 indicate that it has super-solar iron abundance, and is underabundant in magnesium, relative to iron. See discussion in the text.

luminosity-weighted mean metallicity of the central parts of M32, from low-resolution spectrophotometric observations, but O'Connell (1980) was the first to find that such data for the center of M32 could only be matched by requiring an intermediate age population ($\sim$ 5 Gyr) and near-solar metallicity. More recent attempts, based on more sophisticated methods and/or modelling, obtained similar results, with age ranging between 3 and 5 Gyr and [Fe/H] within 0.1 dex from the solar value (e.g. Rose 1994, Jones & Worthey 1995, Vazdekis & Arimoto 1999, Trager et al. 2000, Worthey 2003, Caldwell et al. 2003). These results are confirmed by Figure 8, where we compare the bluer part of the integrated spectrum of M67 that was constructed in Section 3 with the observed integrated spectrum of M32. Some of the most important spectral indices employed in our analysis are indicated in the Figure. As can be seen, the two spectra are very similar. Actually, the integrated spectrum of M32 is in general slightly more strong-lined than that of M67, which suggests a slightly younger age and a slightly higher metallicity.

The latter result can be inspected more quantitatively in Figures 6 and 7, where Lick indices are compared with predictions for single SPs. In order to minimize abundance ratio effects, we first focus on the plots of Balmer lines against Fe indices. According to these plots, the spectroscopic age of M32 is somewhere between 2.0 and 3.5 Gyr, whereas its luminosity-weighted iron abundance is super-solar, with $+0.1 \lesssim$ [Fe/H] $\lesssim +0.3$. These numbers confirm our expectations based on inspection of the spectra of Figure 8.

It is important to bear in mind that the strength of Balmer lines is not solely governed by the temperature and brightness of turnoff stars: other families of hot stars, such as blue stragglers and hot horizontal branch (HB) stars can affect Balmer line strengths, thus hindering their use as age indicators (e.g. Freitas Pacheco & Barbuy 1995, Lee, Yoon & Lee 2000, Maraston et al. 2003). In principle, a small population of hot stars could play a major role in strengthening the Balmer lines in M32, thereby reducing, or eliminating, the necessity for the $\sim$2-3 Gyr old mean population implied by the Balmer line strengths. However, Caldwell et al. (2003) have demonstrated that to explain the enhanced Balmer lines in M32 requires a $\sim$30% contribution from a hot-star component, whether from a blue HB or blue stragglers. On the other hand, they also show that the Ca II index, which levers the strength of Ca II K versus Hϵ + Ca II H, restricts the contribution from hot stars to a level of $\sim$7%. In addition, M32 has the weakest UV upturn in the sample of Burstein et al. (1988), so that its relative number of hot HB stars must be low. In principle, cooler BS stars, that do not make such a strong impact on the above-mentioned Ca II index, could be present in M32, but then they would have to exist in exceedingly large numbers, in fact rivalling the numbers of true MSTO stars. In short, we have reasons to be confident that our Balmer line measurements primarily provide an estimate of the spectroscopic age of M32.

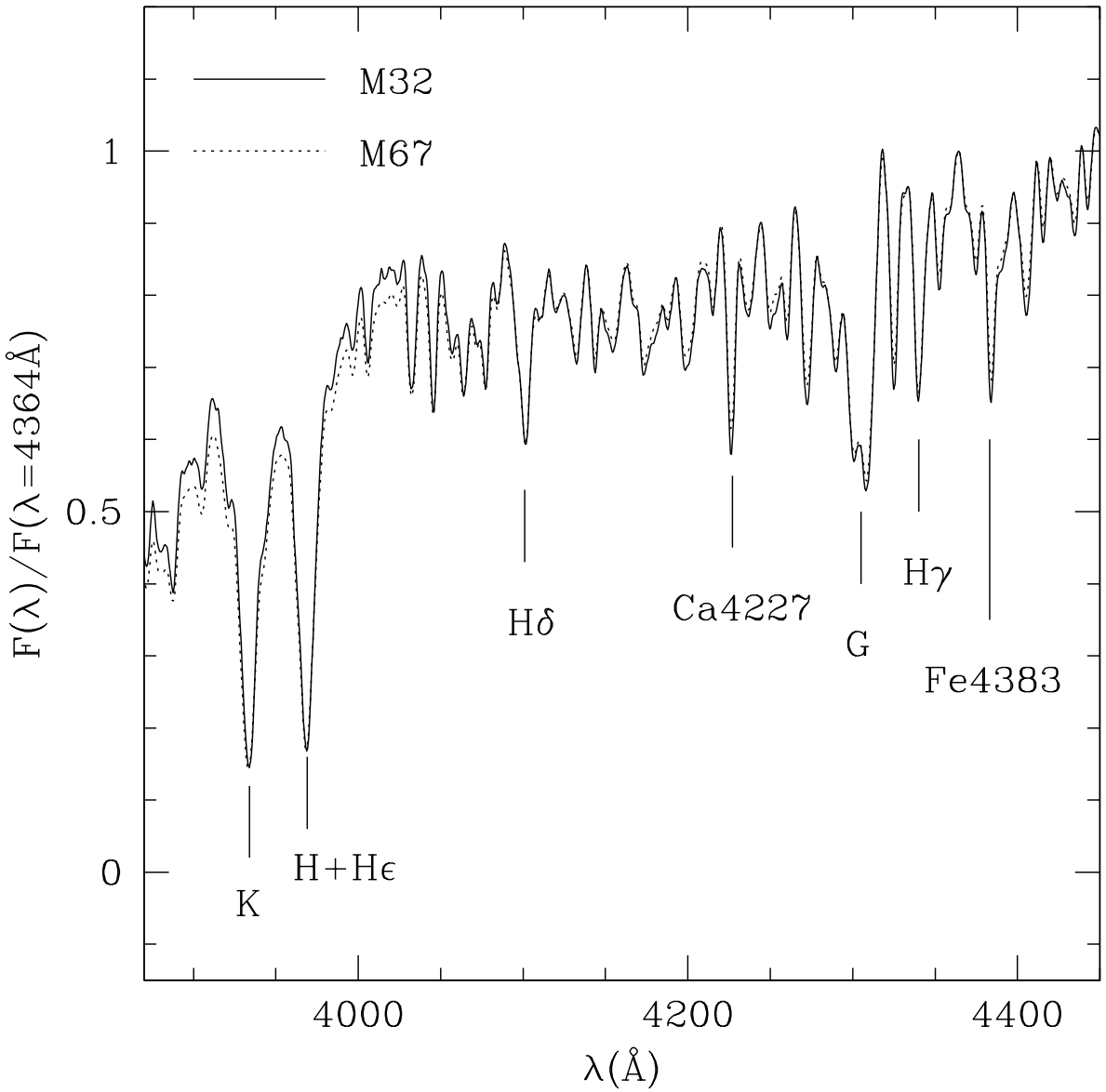

Fig. 8.— Comparison between the integrated spectra of M67 and M32. The spectra are very similar, although M32 looks to be slightly more strong-lined than M67, which suggests that M32 is on average slightly more metal-rich and younger than M67. See discussion in Section 5.

With the above caveats in mind, we now focus on the plots of Balmer lines against CN and Mg indices, in order to assess the abundance ratios of M32. The Mg b index is mostly sensitive to magnesium. In panels (c) and (d) of Figure 7 it is seen that M32 has [Fe/H] $\sim +0.1$ according to $< Fe >$, while, according to Mg b it is about 0.1 dex below the solar metallicity model, which is strongly suggestive of [Mg/Fe] < 0. In the case of the CN indices (panels a and b of Figure 6), in both cases the M32 data fall nearly on top of the [Fe/H]=+0.2 model. Since both CN1 and CN2 are mostly sensitive to the combined effect of nitrogen and carbon abundances, and given the above discussion on the iron abundance of M32, it is likely that M32 has a nearly solar abundance of carbon and/or nitrogen relative to iron.

Abundance ratios can be better assessed in plots of metal index against metal index. Such plots are shown in Figure 9, where we compare the measurements with the model predictions of single stellar populations for [Fe/H] = 0.0 and +0.2. The lines connecting models with same age are omitted in these plots for clarity. In panel (b) it can be seen that while M67 looks like having strictly solar [Mg/Fe], M32 deviates by roughly 3 σ from the model prediction for solar abundance ratios, which confirms the suggestion above that it has [Mg/Fe] < 0. The case for nonsolar abundance ratios for carbon and/or nitrogen is perhaps less convincing, because it depends to some extent on the Fe abundance indicator adopted. In panel (c), where CN1 is plotted against Fe4383, M32 is clearly deviating from the solar ratio models, but less so when CN1 is compared with $< Fe >$ in panel (d) (essentially the same results are obtained in plots involving CN2). We point out that our results agree with those of Worthey (2003) as regards [Mg/Fe], but we are in disagreement when it comes to the abundances of carbon and nitrogen, for which he found an enhancement relative to iron of ~ 0.2 dex.

Finally, we would like to point out an apparent systematic trend of the mean age and metallicity inferred for M32 as a function of wavelength: the resulting age looks lower, and the metallicity looks higher, as we go to bluer indices. According to the $H\beta$ vs. $< Fe >$ plot, the central parts of M32 have luminosity-weighted mean metallicity and age given by [Fe/H] $\sim +0.1$ and ~ 3.5 Gyr. According to the $H\gamma_F$ vs. Fe4383 plot, [Fe/H] is slightly above +0.2, and the mean age is ~ 2.5 Gyr, while in the $H\delta_F$ vs. Fe4383 plot the mean metallicity is even higher and the mean age younger (~ 2.0 Gyr). Even though the spread in the age determinations is relatively small (due to the high age sensitivity of Balmer lines in this age regime), it is significant, given the small errorbars in our measurements. If we assume that the mean age and [Fe/H] of M32 are as given by the $H\beta$ vs. $< Fe >$ plot (3.5 Gyr, +0.1 dex), then the measurements of both $H\gamma_F$ and $H\delta_F$ are off their predicted positions when plotted against Fe4383 by more than 2 σ.

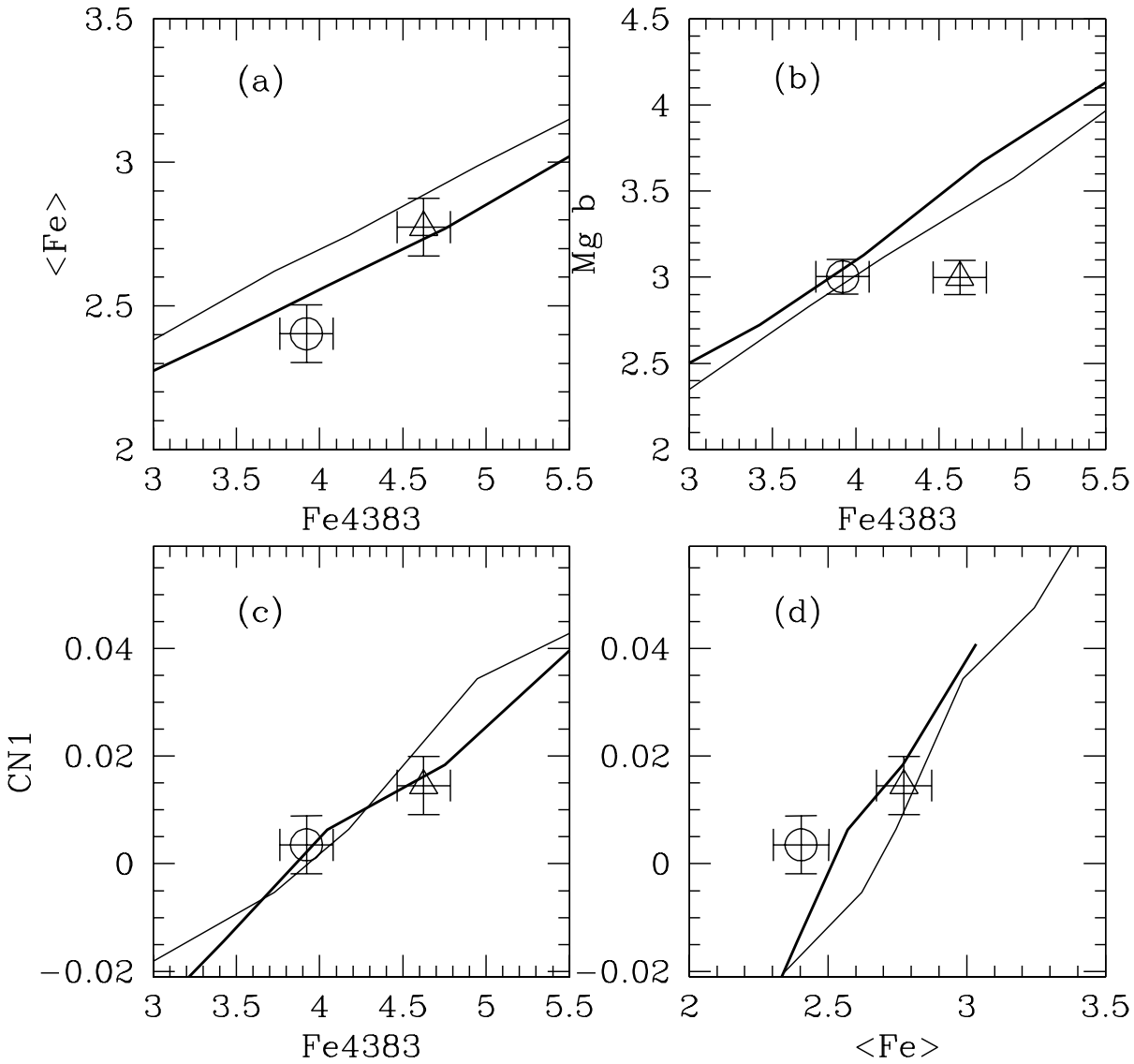

Fig. 9.— The data on M67 and M32 are compared to single SP models on plots involving only abundance-sensitive indices. The symbols adopted are the same as in Figure 6. Such plots are useful to unveil nonsolar abundance ratios. Again, the open triangle and circle represent M67 and M32, respectively. The model lines are for [Fe/H] = 0.0 and +0.2. The former is represented by a thick line. The lines connecting same-age models are omitted for clarity. While M67 is basically consistent with solar in all abundance ratios, M32 appears to have [Mg/Fe] substantially below solar. The combined abundances of C and N appear to be nearly solar in the center of M32.

This result should be contrasted against the case of M67, for which we found essentially the same age for all Balmer lines, and iron abundances according to different Fe indices in agreement to within 0.1 dex. M32 differs from M67 in two basic aspects: 1) It is not a single stellar population, but rather a mix of stars of different metallicities (Grillmair et al. 1996) and possibly different ages; 2) As discussed above, M32 has an abundance pattern that differs from that of the Sun.

A simple calculation shows that a very small fraction of a young ($\sim$ 1.5 Gyr) stellar population on top of an older one can reproduce data for Balmer and Fe lines. The younger stellar population is much brighter in the blue, so that it would affect bluer spectral indices more strongly with the result that the bluer Balmer lines of such a simple composite stellar population would indicate younger ages.

On the other hand, it might be also possible to reproduce the data by applying the method championed by Trager et al. (2000), where the absorption line indices are corrected for varying abundance ratios, based on the computations of synthetic stellar spectra by Trippico & Bell (1995). The latter does not include calculations for $H\delta_F$ and $H\gamma_F$ though, because these indices were defined later, by Worthey & Ottaviani (1997). This is important because we have shown, in Schiavon et al. (2002a), that both $H\gamma_F$ and $H\delta_F$ are influenced by variations in the abundances of carbon and nitrogen, due to the contamination by CN and CH lines. While we cannot correct the higher order Balmer lines for the effects of unknown abundance ratios, we recognize that they might be at least partially responsible for the results of Figures 6 and 7.

It is very hard to disentangle the effect of varying abundance ratios from the potential age mix of stellar populations. As a consequence, when blue indices are involved, it is difficult to apply the method devised by Trager et al. (2000) to assess nonsolar abundance ratios. The reason is that the method essentially seeks the combination of metal abundances that brings the ages and metallicities into agreement according to the different line indices, so that it tends to wash out any effect due to a mix of stellar populations of different ages. In a future paper, we will address this problem in more detail.

6. Conclusions

We have constructed an integrated spectrum of the Galactic cluster M67, from spectroscopic observations of bona fide cluster members. The resulting integrated spectrum was used as a template for stellar population synthesis, through comparison with model predictions for single stellar populations. We constrasted the spectroscopic age and metal abundances

estimated from the SP models with the age obtained from the cluster CMD, and elemental abundances determined in previous works from high dispersion abundance analyses. It is the first time that such models are tested to this level of precision in the solar metallicity, intermediate-age regime. Our SP models were then applied to the study of the integrated spectrum of M32, yielding reliable determinations of the galaxy's light-weighted mean age and metal abundances. We summarize below our main conclusions.

1. Our models for the known age and metal abundances of M67 match very well its integrated spectrum. Adopting the Girardi et al. (2000) theoretical isochrones for solar metallicity and solar abundance ratios, we matched both the color-magnitude data and integrated spectrum of M67, for an age of 3.5 Gyr and solar metallicity, to within 0.5 Gyr and 0.1 dex respectively. Most importantly, we found very good consistency for the ages derived from $H\beta$, $H\gamma$ and $H\delta$. This result demonstrates the remarkable degree of consistency of our models. We also performed a detailed check to see whether our model predictions are consistent with the known elemental abundances of M67 stars. We found that the predictions from SP models for the abundances of iron, carbon, nitrogen and magnesium agree with the elemental abundance analyses of individual stars to within 0.1 dex.

2. The integrated spectrum of M32 is very similar to, though slightly more strong-lined than, that of M67. On the basis of our newly tested models, we perform an analysis of the integrated spectrum of M32, with the aim of estimating its light-weighted mean age and metal abundances. We found that the spectroscopic age of M32 is somewhere between 2 and 3.5 Gyr, depending on the Balmer line adopted. For the mean metal abundances, we found [Fe/H] ranging between +0.1 and +0.4, again depending on the metallicity indicators adopted. For light elements, we found M32 to be underabundant in magnesium relative to iron, with [Mg/Fe] $\sim$ –0.2, whereas the combined abundances of carbon and nitrogen seem to be nearly solar relative to iron. A more in-depth study of the composite nature of the stellar populations in M32 is deferred to a forthcoming paper.

3. Contrary to the case of M67, application of our single stellar population models to the integrated spectrum of the central parts of M32 revealed a systematic effect in the resulting ages and metallicities as a function of wavelength. Use of red indices results in a mean age $\sim$ 1.5 times older and a metallicity $\sim$ 0.3 dex lower than when blue indices are adopted. This result can be due to either the effects of nonsolar abundance ratios on blue absorption indices, and/or to a mix of stellar populations in M32, with different ages.

4. In agreement with previous studies, we found that blue stragglers contribute with an unusually high fraction of the blue integrated light of M67. This result is robust, since our integrated spectrum is constructed on the basis of photometry which is complete down to many magnitudes below the turnoff. We suggest that this result might be due to the

cluster's past history of severe mass segregation, followed by evaporation of low-mass stars.

Calibrating models by comparison with integrated spectra of clusters has become a standard procedure in the field of stellar population synthesis. The nature of the Galactic globular cluster system, and the limitations of our knowledge of the detailed abundance pattern of their constituent stars, has prevented an accurate calibration of such models with the degree of accuracy that is required for many of their applications. The latter is particularly true in the regime of solar metallicity and intermediate ages, which is of great importance in view of its potential application for the study of stellar populations of distant systems, for which the lookback times are more than half the Hubble time. This work is an attempt at filling this gap. Applications of our models to the study of galaxies both nearby and at cosmological distances are currently under way.

We would like to thank S. Faber for enlightening discussions during the course of this investigation. The referee, Guy Worthey, is thanked for comments and suggestions that greatly improved this paper. We also thank Hyun-chul Lee for a careful reading of an earlier version of this manuscript. R.P.S. acknowledges support provided by the National Science Foundation through grant GF-1002-99 and from the Association of Universities for Research in Astronomy, Inc., under NSF cooperative agreement AST 96-13615 (Gemini Fellowship). Support from the NSF, through grant AST-0071198 to the University of California, Santa Cruz and from CNPq/Brazil, under grant 200510/99-1 are also deeply thanked. J.A.R. acknowledges support from NSF grant AST-9900720 to the University of North Carolina

Table 4. Cool giants included in the synthesis of the integrated spectrum of M67 and $T_{\rm eff}$s used to estimate their masses.

ID	$T_{\rm eff}$ (K)	ID	$T_{\rm eff}$ (K)
HD 94705	3350	MMJ-6513	3950
MMJ-6514	3740	MMJ-6515	3950
HD 60522	3900	MMJ-6486	3950
MMJ-6471	3920	MMJ-6470	3960
HD 70272	3930	MMJ-6499	3960
HD 47914	3940	MMJ-6482	3960
HD 62721	3940	MMJ-6495	3960

Table 5. Absorption Line Indices Measured

	$H\delta_F$	$H\delta_A$	CN1	CN2	G4300	$H\gamma_F$	$H\gamma_A$	Fe4383	$H\beta$	$Mg2$	Mgb	Fe5270	Fe5335
M67 (no BS)	0.92	-0.65	0.001	0.030	4.8	-0.33	-4.0	3.9	2.37	0.18	2.9	2.53	2.20
M67 (with BS)	3.05	3.31	-0.078	-0.045	2.6	2.16	0.7	2.4	3.46	0.14	2.3	2.06	1.81
M32	0.75	-1.12	0.015	0.046	4.9	-0.56	-4.5	4.6	2.25	0.21	3.0	2.95	2.60
Error	0.09	0.14	0.005	0.008	0.1	0.05	0.2	0.2	0.09	0.01	0.1	0.06	0.08

Table 6. Lick indices measured in the spectra of field and M67 stars

ID	$H\delta_F$	CN1	CN2	G4300	$H\gamma_F$	Fe4383	$H\beta$	Mg b	Mg 2	Fe5270	Fe5335
HD37216	-0.0927	-0.0268	-0.0090	5.5800	-1.7390	5.0640	1.9310	4.0450	0.1866	2.6840	2.3580
HD47914	-1.3580	0.1929	0.2470	6.0950	-3.6050	8.9290	0.6220	4.6620	0.4279	4.3080	4.3690
HD49178	0.7858	-0.0070	0.0108	5.2630	-0.6413	3.7520	2.6100	3.2390	0.1454	2.1010	1.8940
HD60522	-1.2280	0.1305	0.1837	5.8620	-3.2510	8.7260	0.7104	4.7330	0.4284	4.2310	4.3430
HD61606A	-1.1130	0.0038	0.0308	5.7230	-3.2210	7.5730	0.9142	5.9370	0.3588	3.7920	3.6200
HD62721	-0.9038	0.1198	0.1765	6.0490	-3.0220	7.7080	0.4400	4.8540	0.4132	3.8200	3.7120
HD69582	0.4846	-0.0427	-0.0294	4.9650	-0.6286	4.0670	2.4240	3.3490	0.1475	2.4380	2.0690
HD69830	-0.0913	-0.0208	-0.0053	5.7350	-1.8680	4.9510	1.9740	4.3250	0.1949	2.6830	2.2900
HD70272	-1.4280	0.1288	0.1807	5.8610	-3.0130	8.8740	0.7205	4.2880	0.3889	4.3060	4.3320
HD94705	-0.6903	-0.1174	-0.0824	3.5000	-2.2890	-0.2740	5.0380	14.0800	0.4313	3.4070	1.2200
HD98991	3.3470	-0.1002	-0.0778	1.5110	3.5730	0.8280	4.3510	0.8016	0.0480	1.1230	0.9891
HD106156	-0.1425	0.0264	0.0430	5.6730	-1.8050	5.4120	2.1650	4.4290	0.2197	3.0360	2.6080
HD128987	0.1842	-0.0374	-0.0236	4.9530	-1.0410	4.3020	2.1810	3.7900	0.1631	2.6530	2.2100
HD126511	0.0126	0.0123	0.0278	5.4960	-1.6630	4.9920	2.3380	4.2010	0.1986	2.5700	2.4120
HD136834	-1.1980	0.1275	0.1618	5.9300	-3.5640	7.9070	1.2520	6.4510	0.4054	4.1830	3.8950
HD158614	0.4254	-0.0222	-0.0110	5.3790	-1.1710	4.0860	2.4000	3.5730	0.1599	2.4140	2.1240
HD165341	-0.4514	0.0045	0.0196	5.6020	-2.2010	5.5210	1.7720	4.7960	0.2407	3.2220	2.7730
5041	1.8350	-0.0712	-0.0505	4.1610	1.1570	2.0860	3.1420	1.4940	0.0735	1.7170	1.3170
5059	-0.6574	0.0772	0.0985	6.4420	-2.7460	5.4150	1.6330	3.4310	0.2000	2.9500	2.4030
5118	2.5360	-0.0914	-0.0688	2.9890	2.2230	1.2170	3.5770	1.3260	0.0758	1.3320	1.0400
5169	2.1560	-0.0833	-0.0597	3.6500	1.6450	1.8200	3.4600	1.5350	0.0795	1.5380	1.3140
5191	3.0040	-0.1002	-0.0786	2.2490	2.8480	1.0120	3.8600	1.2530	0.0623	1.3220	1.1000
5228	-0.1325	0.0209	0.0363	6.2920	-2.1600	4.8060	1.7300	3.0820	0.1529	2.5730	2.0500

Table 6—Continued

ID	$H\delta_F$	CN1	CN2	G4300	$H\gamma_F$	Fe4383	$H\beta$	Mg b	Mg 2	Fe5270	Fe5335
5248	2.4470	-0.0860	-0.0652	3.5480	1.7650	1.3220	3.3970	1.3930	0.0838	1.4070	1.1990
5249	2.2360	-0.0822	-0.0638	3.7910	1.4580	2.0730	3.3650	1.8860	0.0899	1.6140	1.3370
5284	2.4350	-0.0896	-0.0691	3.3520	1.9440	1.5680	3.5410	1.2500	0.0718	1.4170	1.1730
5318	-0.5367	0.0583	0.0783	6.2910	-2.6440	5.7050	1.6200	3.6720	0.2010	3.0350	2.5910
5342	2.4070	-0.0882	-0.0683	3.8590	1.5780	1.7010	3.3740	1.5190	0.0850	1.4940	1.1640
5350	0.3455	-0.0233	-0.0069	5.8260	-1.2980	4.5590	2.3520	3.0070	0.1533	2.5630	2.2000
5362	0.7275	-0.0467	-0.0328	5.6220	-0.7988	3.3720	2.3280	2.1620	0.1239	2.0650	1.6160
5451	1.5520	-0.0627	-0.0474	3.5540	0.7303	2.4130	2.2350	1.9260	0.1018	1.8950	1.4650
5544	1.4190	-0.0590	-0.0376	4.8810	0.2851	2.5190	2.6930	2.0140	0.1047	1.7630	1.5410
5571	2.9790	-0.1046	-0.0779	2.5040	2.9570	1.0840	4.1210	0.9612	0.0517	1.3190	1.1960
5583	2.2060	-0.0825	-0.0601	3.6910	1.6270	1.7870	3.3220	1.6920	0.0722	1.5700	1.2890
5586	2.4330	-0.0931	-0.0688	3.1840	2.1150	1.9050	3.5070	1.2550	0.0708	1.4060	1.2950
5643	0.8413	-0.0290	-0.0105	4.7740	-0.2366	3.3870	2.2390	2.5120	0.1412	2.3450	2.0180
5667	3.8030	-0.1166	-0.0924	1.1210	3.8120	0.6684	4.6040	1.1990	0.0626	1.1680	1.0500
5679	2.3330	-0.0872	-0.0662	3.7270	1.7080	1.8900	3.4330	1.4100	0.0767	1.3710	1.2590
5688	2.3600	-0.0883	-0.0635	3.2900	1.9500	1.7650	3.5380	1.5120	0.0789	1.4120	1.3480
5699	2.1560	-0.0762	-0.0557	3.6260	1.5890	1.8640	3.4010	1.5540	0.0812	1.4880	1.3660
5716	3.7310	-0.1166	-0.0910	1.4190	3.8170	0.6320	4.5290	1.1250	0.0577	1.2450	1.1110
5741	3.5250	-0.1098	-0.0828	1.6800	3.3810	0.4970	4.3640	1.2770	0.0729	1.3030	1.0070
5756	0.4934	-0.0192	-0.0015	5.8670	-1.3880	3.9920	2.2090	2.4950	0.1438	2.2780	2.1380
5790	1.9560	-0.0751	-0.0563	3.8440	1.4240	2.0180	3.2710	1.5170	0.0716	1.6810	1.3090
5795	2.3000	-0.0880	-0.0638	3.8310	1.3350	1.8720	3.3840	1.7530	0.0916	1.6410	1.3410
5833	3.5450	-0.1085	-0.0840	0.6459	3.8750	0.5400	4.3300	1.1480	0.0648	1.0540	1.0460

Table 6—Continued

ID	$H\delta_F$	CN1	CN2	G4300	$H\gamma_F$	Fe4383	$H\beta$	Mg b	Mg 2	Fe5270	Fe5335
5853	1.3380	-0.0647	-0.0478	5.0660	0.1488	2.6760	2.8280	1.6980	0.0841	1.8720	1.2700
5855	-0.5064	0.0567	0.0814	6.2290	-2.5850	5.4600	1.5810	3.4320	0.1819	2.7090	2.4010
5927	-0.1161	-0.0139	0.0042	6.1910	-1.8380	4.0610	2.0470	3.0560	0.1669	2.6250	2.1500
5929	1.8280	-0.0715	-0.0521	4.3900	1.0160	2.2430	3.1220	1.4430	0.0758	1.6710	1.3540
5969	2.7860	-0.0898	-0.0680	2.8390	2.4270	1.2450	3.6860	1.2620	0.0506	1.4190	1.2740
5993	1.1720	-0.0494	-0.0339	4.8060	-0.0446	2.7430	2.6520	2.0150	0.1135	1.8920	1.4980
5996	0.6355	-0.0346	-0.0239	5.5530	-0.7603	3.6020	2.4280	2.2500	0.1211	2.0740	1.7290
5997	-0.7729	0.1205	0.1478	6.2870	-2.6590	5.7530	1.5230	3.3980	0.1942	2.9150	2.5600
6089	2.0870	-0.0813	-0.0615	3.8510	1.4750	2.0260	3.2100	1.5350	0.0633	1.6480	1.3260
6107	0.6495	-0.0394	-0.0272	5.2630	-0.7022	3.2150	2.4020	2.1970	0.1223	2.0390	1.7040
6114	-0.6396	0.0471	0.0607	6.3370	-2.4530	5.5260	1.7060	3.3890	0.1808	2.7740	2.3590
6134	2.2270	-0.0872	-0.0637	3.5200	1.5980	1.8430	3.4880	1.5910	0.0891	1.5020	1.2290
6158	1.3580	-0.0649	-0.0489	4.5780	0.6104	2.6430	2.6800	1.9630	0.0940	1.7930	1.5690
6169	-0.5138	0.0632	0.0806	6.0210	-2.5500	5.3930	1.5990	3.3860	0.1934	2.8360	2.5970
6228	2.0570	-0.0855	-0.0689	3.9570	1.3130	1.9620	3.2580	1.3770	0.0657	1.5600	1.2440
6259	-0.9166	0.0757	0.1007	6.4420	-2.8500	5.6510	1.5730	4.0570	0.2143	3.0730	2.4050
6313	2.2710	-0.0868	-0.0654	3.3920	1.8730	1.7610	3.5000	1.4410	0.0748	1.5120	1.1330
6395	1.9910	-0.0806	-0.0597	4.2720	1.0910	2.0080	3.0960	1.9860	0.0891	1.5930	1.3650
6408	0.2703	-0.0144	0.0028	5.7480	-1.2760	4.2950	2.0830	2.8160	0.1345	2.3000	1.9840
6470	-1.4870	0.2358	0.2844	6.2960	-3.4310	7.7730	0.9060	3.6800	0.2921	3.8690	3.4910
6471	-1.1870	0.1540	0.2084	5.8500	-3.2070	8.6350	0.7761	4.3940	0.4100	4.1820	4.3690
6472	-1.1900	0.1644	0.1912	6.7930	-2.8270	5.3920	1.4300	2.6690	0.1739	3.0650	2.5640
6477	2.1780	-0.0835	-0.0606	3.7970	1.4510	1.8820	3.3550	1.5290	0.0851	1.6310	1.3730

Table 6—Continued

ID	$H\delta_F$	CN1	CN2	G4300	$H\gamma_F$	Fe4383	$H\beta$	Mg b	Mg 2	Fe5270	Fe5335
6480	4.0450	-0.1177	-0.0893	0.8838	4.3800	0.8779	4.8870	0.7455	0.0436	1.2260	1.0270
6481	7.0520	-0.2051	-0.1683	-2.9240	7.1090	-0.6073	7.1850	0.0866	0.0205	0.0389	0.0213
6482	-1.3470	0.2099	0.2611	6.2420	-3.3350	7.7600	0.8280	3.8330	0.3172	3.9210	3.5610
6484	3.9380	-0.1190	-0.0912	0.4985	4.2160	0.3073	4.6610	0.8662	0.0595	1.0440	0.8099
6485	-1.2040	0.2296	0.2623	6.7130	-2.9230	6.0340	1.5110	2.8570	0.1915	3.3000	2.8240
6486	-1.3900	0.2418	0.2834	6.3810	-3.4920	7.4740	1.0910	3.6520	0.2707	3.7370	3.3920
6488	-0.3128	0.0549	0.0778	5.8770	-1.7400	4.6280	1.8610	2.7210	0.1600	2.5440	2.2240
6489	-1.2280	0.1916	0.2265	6.5360	-2.8870	6.0840	1.3880	3.3180	0.1968	3.2150	2.6390
6490	9.0460	-0.3158	-0.2714	-3.7640	9.2760	-1.8830	9.0600	0.4973	0.0164	0.2899	0.0941
6491	1.5270	-0.0628	-0.0464	4.1230	1.0880	2.3480	3.0050	1.2600	0.0634	1.6230	1.2550
6492	-1.3510	0.2239	0.2554	6.7100	-2.9540	6.2510	1.5190	2.8350	0.1745	3.2140	2.5730
6494	-1.0970	0.2244	0.2599	6.6090	-2.8540	5.7160	1.5210	2.7620	0.1688	3.1190	2.6600
6495	-1.1850	0.1990	0.2486	6.1260	-3.4330	8.3990	0.6640	3.8390	0.3584	4.1590	4.1790
6497	-1.3540	0.2750	0.3102	6.0460	-2.6810	6.5930	1.4390	3.3610	0.1985	3.4100	2.9380
6499	-1.3530	0.2355	0.2879	6.4090	-3.3460	7.8350	0.9870	3.5970	0.2929	3.8970	3.4580
6501	7.3830	-0.2491	-0.2039	-2.1570	8.0400	-1.3630	7.9410	0.4634	0.0290	0.8123	0.5647
6502	-1.2750	0.1865	0.2135	6.6060	-3.0200	6.3420	1.4180	3.6170	0.2331	3.2620	2.7790
6503	-1.4410	0.2374	0.2736	6.7290	-2.9620	6.1870	1.4620	2.9450	0.1806	3.2220	2.6680
6505	-1.1990	0.1870	0.2184	6.3550	-2.8850	6.4050	1.4870	3.2760	0.2101	3.3190	2.7220
6506	-1.3100	0.2188	0.2536	6.5560	-2.8660	5.9900	1.5470	2.8710	0.1701	3.1120	2.5860
6510	8.9160	-0.3072	-0.2640	-3.4490	9.0830	-1.8710	8.8540	0.6110	0.0198	0.3626	0.2005
6512	-1.3750	0.2205	0.2540	6.5910	-2.9480	5.7710	1.5090	2.7030	0.1632	3.2150	2.6940
6513	-0.9952	0.1809	0.2239	6.4960	-3.0620	6.3080	1.0570	3.2110	0.2281	3.3220	2.8270

REFERENCES

Ahumada, J. & Lapasset, E. 1995, A&AS, 109, 375

Alonso, A., Arribas, S. & Martínez-Roger, C., 1995, A&A, 297, 197

Alonso, A., Arribas, S. & Martínez-Roger, C., 1999, A&AS, 140, 261

Balogh, M.L., Morris, S.L., Yee, H.K.C., Carlberg, R.G. & Ellingson, E. 1999, ApJ, 527, 54

Beasley, M.A., Hoyle, F. & Sharples, R.M. 2002, MNRAS, 336, 168

Brown, J.A. 1987, ApJ, 317, 701

Burstein, D., Bertola, F., Buson, L.M., Faber, S.M. & Lauer, T.R. 1988, ApJ, 328, 440

Carney, B.W., Latham, D.W. & Laird, J.B. 1989, AJ, 97, 423

Carretta, E., Gratton, R.G. & Sneden, C. 2000, A&A, 356, 238

Chaboyer, B., Green, E.M. & Liebert, J. 1999, ApJ, 117, 1360

Caldwell, N., Rose, J.A. & Concannon, K.D. 2003, ApJ, in press, astro-ph/0303345

Cohen, J.G. 1980, ApJ, 241, 981

Colless, M. et al. 2001, MNRAS, 328, 1039

Davidge, T.J. 1991, AJ, 101, 884

Davis, M. et al. 2003, SPIE, 4834, 161

Deng, L., Chen, R., Liu, X,S, & Chen, J.S. 1999, ApJ, 524, 824

Faber, S.M. 1973, ApJ, 179, 731

Fabricant, D., Cheimets, P., Caldwell, N. & Geary, J. 1998, PASP, 110, 79

Fan, X. et al. 1996, AJ, 112, 628

Fisher, D., Fabricant, D., Franx, M., van Dokkum, P. 1998, ApJ, 498, 195

Foy, R. & Proust, D. 1981, A&A, 99, 221

Freitas Pacheco, J.A. & Barbuy, B. 1995, A&A, 302, 718

Friel, E.D. & Boesgaard, A.M. 1992, ApJ, 387, 170

Table 6—Continued

ID	$H\delta_F$	CN1	CN2	G4300	$H\gamma_F$	Fe4383	$H\beta$	Mg b	Mg 2	Fe5270	Fe5335
6514	-0.9137	0.0462	0.0918	5.0840	-2.8110	7.7780	1.3350	6.1520	0.4777	3.9160	3.9860
6515	-1.4070	0.2461	0.2927	6.3500	-3.4810	7.5920	1.0580	3.8170	0.2846	3.8250	3.4950
6516	-1.3610	0.2350	0.2659	6.6360	-3.0710	5.9680	1.5370	2.8610	0.1869	3.2990	2.7320
Errors	0.03	0.007	0.0004	0.005	0.02	0.04	0.04	0.08	0.005	0.02	0.04

Note. — The Id numbers of M67 stars are from Montgomery et al. (1993). The last row lists mean errors estimated as described in Section 2.2.1

Garcia Lopez, R.J., Rebolo, R. & Beckman, J.E. 1988, PASP, 100, 1489

Gibson, B.K., Madgwick, D.S., Jones, L.A., Da Costa, G.S. & Norris, J.E. 1999 AJ, 118, 1268

Gilmore, G., Wyse, R.F.G. & Jones, J.B. 1995, AJ, 109, 1095

Girardi, L., Bressan, A., Bertelli, G. & Chiosi, C. 2000, A&AS, 141, 371

González, J.J. 1993, PhD Thesis, University of California, Santa Cruz

Gorgas, J., Faber, S.M., Burstein, D., Gonzalez, J.J., Courteau, S. & Prosser, C. 1993, ApJS, 86, 153

Goto, T. et al. 2003, submitted to PASJ, astro-ph/0301305

Gratton, R.G., Sneden, C., Carretta, E. & Bragaglia, A. 2000, A&A, 354, 169

Grillmair, C.J et al. 1996, AJ, 112, 1975

Hardy, E., Couture, J., Couture, C. & Joncas, G. 1994, AJ, 107, 195

Hobbs, L.M. & Thorburn, J.A. 1991, AJ, 102, 1070

Hurley, J.R., Tout, C.A., Aarseth, S.J. & Pols, O.R. 2001, MNRAS, 323, 630

Jones, L.A. 1999, PhD Thesis, University of North Carolina

Jones, L.A. & Worthey, G. 1995, ApJ, 446, L31

Kuntschner, H. 2000, MNRAS, 315, 184

Landsman, W., Bohlin, R.C., Neff, S.G., O'Connell, R.W., Roberts, M.S., Smith, A.M. & Stecher, T.P. 1998, AJ, 116, 798

Le Fèvre et al. 2001, in Proceedings of the ESO/ECF/STScI Workshop, Deep Fields, ed. S. Cristiani, A. Renzini, R.E. Williams (Springer), p. 236

Lee, H., Yoon, S. & Lee, Y. 2000, AJ, 120, 998

Lejeune, Th., Cuisinier, F. & Buser, R. 1997, A&AS, 125, 229

Leonardi, A.J. & Rose, J.A. 1996, AJ, 111, 182

Leonardi, A.J. & Rose, J.A. 2003, AJ, in press, astro-ph/0306358

Maeder, A. & Meynet, G. 1991, A&AS, 89, 451

Maraston, C., Greggio, L., Renzini, A., Ortolani, S., Saglia, R.P., Puzia, T.H. & Kissler-Patig, M. 2003, A&A, 400, 823

Montgomery, K.A., Marschall, L.A. & Janes, K.A. 1993, AJ, 106, 181

Nissen, P.E., Twarog, B.A. & Crawford, D.L. 1987, AJ, 93, 634

O'Connell, R.W. 1980, ApJ, 236

Poggianti, B.M., Bridges, T.J., Komiyama, Y., Yagi, M., Carter, D., Mobasher, B., Okamura, S. & Kashikawa, N. 2003, ApJ, in press, astro-ph/0309449

Puzia, T.H., Saglia, R.P., Kissler-Patig, M., Maraston, C., Greggio, L., Renzini, A. & Ortolani, S. 2002, A&A, 395, 45

Rose, J.A. 1984, AJ, 89, 1238

Rose, J.A. 1985a, AJ, 90, 787

Rose, J.A. 1985b, AJ, 90, 803

Rose, J.A. 1994, AJ, 107, 206

Schiavon, R.P. & Barbuy, B. 1999, ApJ, 510, 934

Schiavon, R.P., Barbuy, B. & Bruzual A.,G. 2000, ApJ, 532, 453

Schiavon, R.P., Faber, S.M., Castilho, B.V. & Rose, J.A. 2002, ApJ, 580, 850

Schiavon, R.P., Faber, S.M., Rose, J.A. & Castilho, B.V. 2002, ApJ, 580, 873

Shetrone, M.D. & Sanquist, E.L. 2000, AJ, 120, 1913

Spinrad, H. & Taylor, B.J. 1971, ApJS, 22, 445

Tautvaisiene, G., Edvardsson, B., Tuominen, I. & Ilyin, I. 2000, A&A, 360, 499

Taylor, B.J. 1980, AJ, 85, 242

Trager, S.C., Faber, S.M., Worthey, G. & González, J.J. 2000, AJ, 120, 188

Tran, K.H., Franx, M., Illingworth, G., Kelson, D. & van Dokkum, P. 2003, ApJ, in press, astro-ph/????

Tripicco, M.J. & Bell, R.A. 1995, AJ, 110, 3035

Vazdekis, A. & Arimoto, N. 1999, ApJ, 525, 144

Vazdekis, A., Salaris, M., Arimoto, N. & Rose, J.A., 2001, ApJ, 549, 274

Worthey, G. 2003, AJ, submitted

Worthey, G. & Ottaviani, D.L. 1997, ApJS, 111, 377

Worthey, G., Faber, S.M., González, J.J. & Burstein, D. 1994, ApJS, 94, 687

York, D.G. et al. 2000, AJ, 120, 1579